Outflows in AGN/Starburst-Composite Ultraluminous Infrared Galaxies[1][2][3]

David S. Rupke, Sylvain Veilleux

Department of Astronomy, University of Maryland, College Park, MD 20742

drupke@astro.umd.edu, veilleux@astro.umd.edu

and

D. B. Sanders

Institute for Astronomy, University of Hawaii, 2680 Woodlawn Drive, Honolulu, HI 96822

sanders@ifa.hawaii.edu

ABSTRACT

Galactic superwinds occur in almost all infrared-luminous galaxies with star formation rates (SFRs) above 10 $M_\odot$ yr^{-1}, as shown by studies of the Na I D interstellar absorption line. We demonstrate that this result also applies to ultraluminous infrared galaxies (ULIRGs) which host an active galactic nucleus (AGN) embedded in a strong starburst (SFR $\gtrsim$ 100 $M_\odot$ yr^{-1}) by studying a sample of 26 Seyfert ULIRGs in Na I D. The infrared luminosity of these galaxies is powered jointly by the AGN and starburst. We find that there are hints of the influence of the AGN on outflows in Seyfert 2/starburst composites, but the evidence is not yet statistically conclusive. The evidence we find is lower wind detection rates (i.e., wind opening angles) in Seyfert 2 ULIRGs than in galaxies of comparable L_{IR}, higher velocities than in galaxies of comparable SFR, and

correlations between the neutral gas and the ionized gas in the extended narrow-line region. Though the AGN probably contributes to the outflows in Seyfert 2 ULIRGs, its momentum and energy injection is equal to or less than that of the starburst. Similarly, the outflow mechanical luminosity (energy outflow rate) per unit radiative luminosity is the same for starburst and Seyfert 2 ULIRGs. In the nuclei of Seyfert 1s, we observe small-scale outflows that are powered solely by the AGN. However, in Mrk 231, we observe both a high-velocity, small-scale and low-velocity, extended outflow. The latter may be powered by a starburst or radio jet. These large-scale, lower-velocity outflows certainly exist in other Seyfert 1 ULIRGs, but they are washed out by the light of the nucleus.

Subject headings: galaxies: Seyfert — galaxies: active — galaxies: absorption lines — infrared: galaxies — ISM: jets and outflows — ISM: kinematics and dynamics

1. INTRODUCTION

Mechanical and radiative feedback from active galactic nuclei (AGN) are beginning to gain attention as important astrophysical processes. By definition, active galactic nuclei have strong radiation fields. They typically possess outflows in the form of spatially-resolved jets on parsec to kiloparsec scales, in both radio-loud (e.g., Zensus 1997; Worrall & Birkinshaw 2004) and radio-quiet (e.g., Morganti et al. 1999; Nagar, Falcke, & Wilson 2005) objects. UV and X-ray absorption-line probes also point to wide-angle outflows originating from AGN on scales of tens of pc or less (Crenshaw, Kraemer, & George 2003; Crenshaw & Kraemer 2005; McKernan, Yaqoob, & Reynolds 2005, and references therein). This radiation and outflowing gas deposit mass and energy into the surroundings of the AGN, including the ISM of the galaxy in which the AGN resides and the larger-scale intergalactic and intracluster media.

The possible effects of AGN feedback are numerous; we here list a few important ones. Radiation from quasars almost certainly helped to reionize the universe at high redshift, though the strength of their contribution is yet uncertain (Fan et al. 2004). Outflows from AGN have recently been invoked as global heat (or entropy) sources for the intracluster medium (ICM) at both small and large radii (e.g., Reynolds, Heinz, & Begelman 2002; Roychowdhury et al. 2004, and references therein). On more local scales, jets from AGN at both low and high redshift have been shown to induce star formation by shocking dense clouds of gas (e.g., Bicknell et al. 2000; Mould et al. 2000; Rejkuba et al. 2002; Fragile et al. 2004). Very recently, Springel, Di Matteo, & Hernquist (2005) have suggested that AGN feedback can quench star formation in massive, gas-rich mergers, creating a population of

very red ellipticals and possibly explaining the observed bimodal color distribution observed in deep galaxy surveys (e.g., Kauffmann et al. 2003; Weiner et al. 2005).

This work will focus on wide-angle outflows (though this will also lead us to some discussion of jets). By 'wide-angle outflows', we mean outflows that subtend large solid angles as seen from the wind's origin. They are thus structurally distinct from jets, in that jets are highly collimated. The narrow-line regions (NLRs) and host galaxies of AGN often host large-scale, wide-angle outflows. (For a recent summary, see Veilleux, Cecil, & Bland-Hawthorn 2005.) Radio continuum, optical emission-line, and X-ray emission probes reveal extended structures and kinematic evidence for these types of outflows in many local Seyfert galaxies. A number of surveys have shown that outflows are common, though they disagree on some of the details and on whether or not the AGN drives the outflow if a starburst is also present (Baum et al. 1993; Colbert et al. 1996a,b, 1998; Levenson, Weaver, & Heckman 2001a,b). More intensive studies of individual objects are quite numerous (e.g., Cecil, Bland, & Tully 1990 [NGC 1068]; Lindblad 1999; Veilleux et al. 2003 [NGC 1365]; Veilleux, Shopbell, & Miller 2001; García-Lorenzo, Arribas, & Mediavilla 2001 [NGC 2992]; Veilleux et al. 1999a; Iwasawa et al. 2003 [NGC 4388]). The scales of these structures often extend outside of the NLR (i.e., $r \gtrsim 1$ kpc) and are comparable to those found in starburst galaxies.

However, large-scale, wide-angle winds in Seyferts are not identical to those found in starbursts. For instance, the large-scale radio structures in Seyferts do not typically line up with the galaxy's minor axis (Colbert et al. 1996b). However, neither do they align with the nuclear 'linear' radio structure (Baum et al. 1993). Since the large-scale structures are wide-angle winds, and the nuclear structures are jet-like, this implies that the jets from the supermassive black hole accretion disk do not directly drive the large-scale winds (though they may indirectly by injecting energy into the ISM; e.g., Schiano 1985). Furthermore, the X-ray emission in these galaxies is thermal, rather than non-thermal synchrotron as expected in a relativistic plasma that could accompany an AGN wind or jet (Colbert et al. 1998; Levenson et al. 2001a,b).

Different authors have drawn different conclusions about whether or not the AGN powers the large-scale winds in Seyfert 2s. Levenson et al. (2001a,b) argue for a starburst origin from X-ray imaging and spectroscopy, as do Baum et al. (1993) from their radio survey. However, the former sample contains only Seyfert/starburst composites. In a less biased, multi-wavelength survey, Colbert et al. (1996a,b, 1998) argue for AGN jet-heating of the galaxy ISM as the driving force of the outflow. AGN influence is also invoked in various individual cases (see above references for individual galaxies).

In galaxies containing both a starburst and a Seyfert nucleus, the confusion over the

source of the outflow arises in the fact that large-scale, wide-angle outflows are also common features of starbursting galaxies. Outflows of neutral gas and dust stretching over kiloparsec scales are found in almost all massive, starbursting galaxies in the local universe (Rupke, Veilleux, & Sanders 2005a,b; hereafter Papers I and II). These outflows reach projected velocities up to 600 km s^{-1} (and >1000 km s^{-1} in one galaxy), though most of the gas is at lower velocities ($100 - 200$ km s^{-1}). A large fraction (43/78) of the galaxies we studied in Papers I and II were starburst-dominated ultraluminous infrared galaxies (ULIRGs), which have total infrared (and bolometric) luminosities greater than 10^{12} $L_\odot$. Many ULIRGs also host a strong AGN along with a strong starburst. Mid-infrared spectroscopy with the *Infrared Space Observatory* (*ISO*) suggests that these AGN account for $60 - 80\%$ of the galaxies' bolometric luminosities (Lutz, Veilleux, & Genzel 1999).

These starburst/Seyfert composites are the focus of the current paper. Based on our study of pure starbursts in Papers I and II, we hypothesize that most Seyfert ULIRGs, with star formation rates (SFRs) greater than 100 M$_\odot$ yr^{-1}, will also host starburst-driven winds. However, the dominant AGN in these galaxies could have a measurable impact on the outflow. By comparing the properties of outflows in Seyfert 1s and 2s with those in starburst-dominated ULIRGs, we can search for evidence that these outflows are partially powered by the central AGN.

The 26-galaxy sample we discuss in this paper consists of 17 Seyfert 2 ULIRGs, 3 Seyfert 2 LIRGs (with $10^{11} < L_{IR}/L_\odot < 10^{12}$), and 6 Seyfert 1 ULIRGs observed in the Na I D $\lambda\lambda$5890, 5896 doublet absorption feature at moderately high spectral resolution ($65 - 85$ km s^{-1}). This feature probes neutral gas, due to its low ionization potential (5.1 eV). For $z < 0.5$, it is found in the optical. Its high interstellar abundance makes it a good probe of the ISM. Blueshifted velocity components in Na I D unambiguously indicate the presence of outflowing gas.

The organization of this paper is as follows. In §2, we discuss our sample selection and observations and summarize the data analysis procedures. We discuss the outflow properties of Seyfert 2 ULIRGs in §3 and compare to the properties of outflows in infrared-luminous starbursts. We also study correlations between emission and absorption lines. In §4 we discuss outflows in Seyfert 1 ULIRGs. Mrk 231 is presented as a special case in §5, since it possesses both a small-scale and large-scale wind. We discuss further issues in §6, including the location of the absorbing gas, outflow/galaxy correlations, the global covering factor of the outflows, the gas escape fraction, and the scientific context. §7 summarizes and concludes.

For all calculations, we assume present-day values for the cosmological parameters of $H_0 = 75$ km s^{-1} Mpc^{-1} and the standard $\Omega_m = 0.3$, $\Omega_\Lambda = 0.7$ cosmology. All wavelengths

quoted are vacuum wavelengths (except those used as labels for spectral lines) and are generally taken from the NIST Atomic Spectra Database[1]. (The vacuum wavelengths of Na I D are 5891.58 and 5897.55 Å.)

2. SAMPLE, OBSERVATIONS, AND ANALYSIS

2.1. Sample

The primary selection criteria for our sample are that the galaxies be optically classified as Seyfert galaxies and have high infrared luminosities ($L_{IR} \gtrsim 10^{12} L_\odot$). Our sample of infrared-selected Seyferts consists of 23 ULIRGs and 3 LIRGs. The only redshift criterion is $z < 0.50$, so that Na I D is not redshifted into the near-infrared and the galaxy is not too faint. All but four galaxies have redshifts less than 0.25; the others have redshifts in the range $0.25 < z < 0.50$.

Most galaxies are selected from 1 Jy survey (Kim & Sanders 1998), which is a complete flux-limited sample of local ULIRGs observed by the *Infrared Astronomical Satellite* (*IRAS*). Spectral types are available from low-resolution spectra (Veilleux, Kim, & Sanders 1999b). Objects were chosen from this catalog purely on the basis of observability. For Papers I and II we also observed galaxies from the FIRST/FSC sample (Stanford et al. 2000); by selection, these galaxies have been detected in both the infrared and the radio. They also have faint infrared fluxes. We selected galaxies from this sample that were neither too compact (to decrease the chances of observing a Seyfert 1) nor too faint (based on their K-band fluxes). We classified several of these galaxies as Seyfert 2s (see below) and thus include them in the present sample. One object (F04210+0401, a galaxy with a known radio jet) is neither a 1 Jy or FIRST/FSC source; it is, however, infrared-luminous.

Table 1 lists the basic properties of the galaxies in our sample. These properties are measured or taken from other sources as described in Paper I (see also the table caption).

2.2. Observations

Our observations were obtained during several observing runs at three different telescopes. The observing runs, exposure times, and slit position angles are listed for each object in Table 1.

---

[1]http://physics.nist.gov/cgi-bin/AtData/main_asd

Several faint galaxies were observed with the Echellette Spectrograph and Imager (ESI; Sheinis et al. 2002) on Keck II. Using echellette mode, we covered the wavelength range $4000 - 11000$ Å in one exposure at a spectral resolution of 65 km s^{-1} FWHM. Data were obtained for two targets with the Red Channel Spectrograph on the MMT, also with an echellette grating. We used a different setup for each run; during the 2002 December run, we covered the wavelengths $4500 - 10200$ Å, and during the 2003 June run, we covered the wavelengths $4300 - 8800$ Å. In each case we used a $1''$ slit to achieve a resolution of 87 km s^{-1}.

Much of our data were obtained at the Kitt Peak 4m using the R-C Spectrograph and a moderate-resolution grating (the KPC-18C, in first order). With this spectrograph we observed 1700 Å in one exposure, allowing us to obtain both the Na I D line and the Hα/[N II] complex at once. We used the GG-475 or GG-495 blocking filters on the R-C Spectrograph and obtained an average resolution of 85 km s^{-1} with a $1''\!.25$ slit.

2.3. Star Formation Rates

The galaxies in our sample possess both an AGN and a strong starburst. For comparison with infrared-luminous galaxies that only contain a strong starburst, we compute the star formation rates of the Seyfert ULIRGs. To do so, we modify the relation between infrared luminosity and star formation rate (Kennicutt 1998) to include a factor α that is equal to the fraction of the infrared luminosity powered by star formation:

$$\mathrm{SFR} = \alpha \; \frac{L_{\mathrm{IR}}}{5.8 \times 10^9 \; L_\odot}. \tag{1}$$

We recognize that α is not a well-constrained quantity, either globally or for individual sources. However, infrared spectroscopy suggests that the AGN is dominant in Seyfert ULIRGs (Genzel et al. 1998; Lutz et al. 1999). Based on these observations, we assign different values of α for different subsets of galaxies. For the Seyfert 1 galaxies in our sample, and a few Seyfert 2s that show either broad lines in the near-infrared or faint broad lines in the optical (see the next section), we assume $\alpha = 0.3$. For the rest of the Seyfert 2s, we assume $\alpha = 0.4$. For reference, we assumed $\alpha = 0.8$ for starburst ULIRGs and $\alpha = 1$ for starbursts with $\log[L_{\mathrm{IR}}/L_\odot] = 10 - 12$ (which we label IRGs, or infrared galaxies; Paper II). Small increases in α ($\lesssim 50\%$) for the Seyfert 2s will not change the conclusions of this study.

2.4. Spectral Types

Each of the galaxies in our sample has a Seyfert 1 or 2 optical spectral classification. These classifications are based on low-dispersion spectroscopy (Kim, Veilleux, & Sanders 1998; Veilleux et al. 1999b) or on our spectra. In confirmation of this classification, we note that four of the galaxies in this subsample were observed in the mid-infrared with *ISO* and are classified as AGN (Lutz et al. 1999). Five to ten Seyfert 2 galaxies in our sample also show evidence for an AGN in the near-infrared, either by the presence of a broad line in Paα or strong [Si VI] 1.962 μm emission (Veilleux, Sanders, & Kim 1999c).

Brief comments are in order regarding the spectral types of a few galaxies. F08526+3720 possesses a faint broad-line region (BLR) in Hα but not Hβ, suggesting it is a Seyfert 1.9 galaxy. We also observe a faint BLR in Hα in F04210+0401 (a galaxy with a large radio jet), though the galaxy is classified as a Seyfert 2 in the literature. We put these galaxies in the Seyfert 2 category despite the visible broad lines.

A final special case is F05189−2524. This optical Seyfert 2 has an optically-obscured BLR and has been shown to host a dominant AGN (Veilleux et al. 1999c). Furthermore, the strength of its 7.7 μm PAH feature (Laureijs et al. 2000) is identical to that of Mrk 231 (Genzel et al. 1998), an optically-classified Seyfert 1. However, for the purposes of this paper we keep the optical spectral type of Seyfert 2.

In all, our sample contains six bona-fide Seyfert 1s, two Seyfert 1.9s with faint BLRs in Hα (which we label Seyfert 2s in this paper), and eighteen other Seyfert 2s.

Three of these Seyferts have double nuclei, and one is a triple nucleus system (F13443+0802). In each case, only one of the nuclei is a Seyfert 1 or 2, and we have derived spectral classes for the other nuclei when the [O III] λ5007 line is available. For simplicity, we subsume the absorption properties of these non-Seyfert nuclei into our analysis.

2.5. Analysis

Paper I describes the details of the spectral extraction and Na I D fitting procedure. From the spectra, we extract as much of the galaxy continuum light as possible, stopping when further extraction harms the signal-to-noise ratio of the extracted spectra. We fit multiple velocity components to the Na I D feature in each object. We assume Gaussians in optical depth, which translates into observable non-Gaussian intensity profiles for optical depths greater than unity. We also fit a constant covering fraction for each velocity component. The results of the fitting are listed in Table 2.

A wind 'detection' is a velocity component with $\Delta v \equiv v_{comp} - v_{sys} < -50$. We also require a 2σ threshold in the measurement uncertainty, such that $|\Delta v| > 2\ \delta(\Delta v)$; this excludes only one source (F17179+5444). These criteria are chosen because of uncertainty in both the outflow velocity and the galaxy's systemic velocity. We compute the 'maximum' velocity in each galaxy, Δv_{max}, equal to the central velocity of the most blueshifted component plus one-half its full-width at half-maximum. We also compute the central velocity of the outflowing component with the highest column density, Δv_{maxN}.

Our physical model is described in detail in Papers I and II. For each galaxy, we compute hydrogen column densities from those of Na I assuming standard Galactic depletion and an ionization fraction of 0.90. Rather than assume solar metallicity, we use the near-infrared luminosity-metallicity relation (Salzer et al. 2005); this results in an average metallicity in our sample of two times solar. (Most of the K'-band magnitudes used to compute the metallicity are corrected for nuclear point source contribution, and thus are not contaminated by the AGN (Veilleux, Kim, & Sanders 2002).) A simple model of a mass-conserving free wind is used to estimate the gas mass, momentum, and energy in the wind, as well as their outflow rates.

There are two differences between the starburst and Seyfert analyses. One is the assumed global covering factor, $\Omega/4\pi$. In our model, we assume $\Omega/4\pi = D\ C_f$ (Paper II and Crenshaw et al. 2003), where D is the detection rate for the sample and C_f is the covering fraction for each velocity component. For the Seyferts, $D = 0.5$, which differs from the values of 0.4 and 0.8 used for the starburst IRGs and ULIRGs, respectively. The second difference is the assumed radius of the absorbers. For the Seyfert 2s, we use the same value of $r = 5$ kpc as for the starbursts. However, we assume $r = 10$ pc for the Seyfert 1s. See §§6.1 and 6.3 for more details.

3. OUTFLOWS IN SEYFERT 2 ULIRGS

3.1. Outflow Properties

In Figure 1, we display the Na I D lines in the 20 Seyfert 2 galaxies in our sample with our fits to the lines superimposed. Tables 2 and 3 list the measured properties of each Na I D velocity component and of the outflow in each galaxy, respectively. Table 4 lists the average outflow properties in this subsample alongside those of starburst IRGs and $z < 0.25$ ULIRGs from Paper II. (We ignore the 13 ULIRGs from Paper II with $0.25 < z < 0.50$, since they are typically higher in luminosity than the other ULIRGs and may have slightly different properties.)

3.1.1. Detection Rate

We detect absorbers blueshifted by more than 50 km s^{-1} in half of Seyfert 2s (45±11%). As we discuss in §6.3, this detection rate reflects the geometry of the outflows, and thus most or all Seyfert 2 ULIRGs contain large-scale, wide-angle outflows.

Other studies produce widely varying detection rates. Applying our threshold to the sample of Heckman et al. (2000), there are winds in 3 of 6 Seyfert 2s, a result identical to ours. Optical investigations show a detection rate of $\gtrsim$25% (Colbert et al. 1996a), while radio imaging studies show much higher incidences ($\sim$60$-$90%; Baum et al. 1993; Colbert et al. 1996b). Low-resolution X-ray images of starburst/Seyfert 2 composites also show evidence of extended emission in most galaxies (Levenson et al. 2001a,b). If outflows really do occur in all Seyfert 2 ULIRGs, these differences are attributable to the different phases of the ISM that these studies probe, as well as their varying sensitivities.

The median star formation rate of our Seyfert 2 ULIRGs (120 M$_\odot$ yr^{-1}) is in between those of the IRG subsample (40 M$_\odot$ yr^{-1}) and low-z starburst ULIRG subsample (225 M$_\odot$ yr^{-1}) from Papers I and II. The detection rate in Seyfert 2s is much closer to that of the IRGs, however (43%, 45%, and 80% for the IRGs, Seyfert 2 ULIRGs, and low-z starburst ULIRGs, respectively, each with a 10% error).

3.1.2. Velocities

In Seyfert 2s, the median velocities of the highest column density gas, Δv_{maxN}, and maximum velocity, $\Delta v_{max} \equiv \Delta v - \text{FWHM}/2$ (computed for the most blueshifted component), are 220 and 456 km s^{-1}, respectively. There is one Seyfert 2 with Δv_{maxN} and $\Delta v_{max} >$ 1000 km s^{-1}: F05024$-$1941.

Tables 4 and 5 compare average properties of outflows in Seyfert 2s with those in starburst galaxies from Paper II. In Table 4, we classify the galaxies according to SFR and AGN activity. In Table 5, we subdivide by spectral type. (The Seyfert 2 velocities in Table 4 are different from those in Table 5 because in the former we list galaxy properties, which may contain non-Seyfert nuclei, while in the latter we limit ourselves to Seyfert nuclei.)

Our subsamples reveal a hierarchy in the median values of Δv_{max} and Δv_{maxN}, such that as one moves from IRGs to low-z ULIRGs to Seyfert 2s, or from H II galaxies to LINERs to Seyfert 2s, the velocities and variances increase. In Figures 2 and 3, we compare the full distributions of Δv_{max} and Δv_{maxN} among our subsamples. Statistical comparisons of these distributions do not fully confirm this hierarchy of velocities. In Table 6, we list the

results from comparing each subsample with the others using both Kolmogorov-Smirnov and Kuiper tests. The K-S test is weighted in favor of differences in the mean, while the Kuiper test is less biased. We print in bold face those comparisons for which the likelihood of two distributions sharing the same parent distribution is less than 10% as determined from *both* tests.

UV data may also indicate higher outflow velocities in some Seyfert 2s than in starbursts, but the evidence is not conclusive due to the number of galaxies observed. (Though many Seyfert 1s have been studied in the UV with the *Hubble Space Telescope* [*HST*] and the *Far-Ultraviolet Spectroscopic Explorer* [*FUSE*], few Seyfert 2s have been.) Outflowing gas has also been observed in the ultraviolet in three Seyfert 2s that are infrared-luminous ($\log[L_{\mathrm{IR}}/L_\odot] = 10.6 - 11.4$) using blueshifted interstellar absorption lines and redshifted Lyα emission lines (González Delgado et al. 1998b). The observed central velocities relative to systemic are $200 - 700$ km s^{-1}. These velocities are similar to those observed in the UV in three infrared-luminous starbursts ($\log[L_{\mathrm{IR}}/L_\odot] = 10.3 - 11.5$), whose blueshifted absorption lines and redshifted Lyα lines have central velocities of $200 - 500$ km s^{-1} (González Delgado et al. 1998a).

Only sample is as yet too small to fully confirm or deny the existence of velocity trends. We conclude that the evidence for higher neutral gas velocities in infrared-luminous Seyfert 2s than in starbursts is highly suggestive but not yet compelling. However, comparing the Seyfert 2 ULIRGs with the starburst IRGs may demonstrate the influence of AGN more conclusively – see §6.7.

3.1.3.   Other Outflow Properties

Our outflow model and the relevant equations for computing the outflow's column density, mass, mass outflow rate, momentum, momentum outflow rate, energy, and energy outflow rate are discussed in detail in Papers I and II. We assume an absorber radius of 5 kpc (§§2.5 and 6.1), an ionization fraction of 0.90, and standard Galactic depletion, and use the luminosity-metallicity relation to estimate metallicity. These quantities and their median values, as well as Na I D equivalent width, optical depth, covering fraction, Doppler parameter, and column density, are listed in Tables $1 - 4$.

We find no statistically significant differences in these outflow properties between infrared-luminous Seyfert 2s and starbursts. The median mass, mass outflow rate, and energy are large, as in starburst galaxies. We measure median values of $M = 10^{8.8}$ M$_\odot$, $dM/dt = 18$ M$_\odot$ yr^{-1}, and $E = 10^{57.0}$ ergs. However, these values can go as high as $10^{9.3}$ M$_\odot$,

300 $M_\odot$ yr^{-1}, and $\sim 10^{58}$ ergs. We have chosen a simple model and assumed several quantities; these values should be treated with some caution.

The median energy outflow rate, or mechanical luminosity, of the neutral gas in Seyfert 2 ULIRGs ($10^{42.2}$ erg s^{-1}) is comparable to that in starburst ULIRGs ($10^{42.2}$ erg s^{-1}) and starburst IRGs ($10^{41.6}$ erg s^{-1}). The average mechanical luminosity (dE/dt) per unit radiative luminosity ($L_{\rm IR}$) is thus the same for each subsample, at $\sim 5 \times 10^{-4}$.

3.2.   Emission-Line Properties

3.2.1.   Blue Emission-Line Asymmetries

In AGN, emission-line profiles with blue-asymmetric wings are a common and well-documented phenomenon (e.g., De Robertis & Osterbrock 1984, 1986; Veilleux 1991a,b,c; Whittle 1992a,b,c). The atoms producing these lines are located in the narrow-line region (the NLR, within a few hundred pc of the nucleus; Veilleux 1991c). The galaxy's, and especially the bulge's, gravitational potential clearly influences the dynamics of the NLR (Veilleux 1991b; Whittle 1992a,b; Nelson & Whittle 1996). However, outflowing gas is also a common feature of NLR models (e.g., Veilleux 1991c, and references therein), which may help to explain the observed blue-asymmetric emission-line wings. There are several lines of evidence for NLR outflow. High-ionization lines tend to show more blueward asymmetry (and higher velocities) than low-ionization lines (De Robertis & Osterbrock 1984; Veilleux 1991c), and the base of these blue-asymmetric profiles are less correlated with galaxy properties than the core of the profiles (Nelson & Whittle 1996). Furthermore, in galaxies with strong radio emission and linear radio structures (i.e., jets), there is an additional high-velocity kinematic component seen in [O III] $\lambda 5007$ that indicates the influence of the collimated outflow of radio plasma (Veilleux 1991c; Whittle 1992b,c; Nelson & Whittle 1996; Veilleux et al. 2005).

In emission lines, however, outflow is not always distinguishable from radial inflow. Blueshifted absorption lines are thus useful in that they are an unambiguous indicator of outflow. Finding a distinct correlation between neutral absorbing and ionized emitting lines, the latter arising in the NLR in Seyferts, would illuminate not only NLR models but also show that the AGN is playing a role in the neutral outflow.

In Figure 4, we plot the Na I D line along with [N II] $\lambda\lambda 6548$, 6583 and/or [O III] $\lambda 5007$ (when available) for the galaxies in which we observe emission lines whose blue and red wings have asymmetric profiles (i.e., one has a higher maximum velocity and/or more flux than the other). As expected, we observe emission lines in which the blue wing has a higher maximum velocity and/or more flux than the red wing in [O III] $\lambda 5007$ and/or [N II] $\lambda\lambda 6548$, 6583 in

15 of 20 Seyfert 2 nuclei, or 75%. We hereafter refer to this blueward asymmetry as BELA, for blue emission-line asymmetry. (Note that for four nuclei, we used low-dispersion spectra from Veilleux et al. 1999b to look for asymmetries in [O III] λ5007.) This compares favorably with the result of Veilleux (1991c), who observe this phenomenon in 10 of 16 Seyfert galaxies, or 63%. It is much larger than the number of infrared-luminous starburst nuclei with BELA (16 of 87, or 18%; Paper II). We also observe redward asymmetries in the emission-line wings of two galaxies (F01436+0120 and Z03150−0219). In F01436+0120, there is a blue wing which has much higher velocities than the red wing, although it carries less flux. We thus include it in the BELA category, as well.

The percentage of nuclei with neutral outflows that also show BELA is high in Seyfert 2s, at 88% (7 of 8 nuclei), much higher than the percentage of starburst nuclei with winds and BELA (24%, or 11 of 45). Note that these percentages are close to the detection rate of BELA in each case. Conversely, the percentage of galaxies with BELA which also have winds is comparable to the detection rate of winds in both cases (69% for starbursts, 47% for Seyfert 2s). This zeroth-order test indicates no strong association of BELA in emission lines and neutral outflows.

3.2.2. Neutral and Ionized Gas

To further explore the relation between neutral outflowing and ionized gas, in Figures 5 and 6 we plot the full-width at half-maximum (FWHM) and full-width at 20% of maximum (FW20) of the [O III] λ5007 line as a function of Δv_{max} and Δv_{maxN} in Seyfert 2s and starbursts. We plot these quantities against each other for all nuclei with winds and only for those in which we observe winds and BELA. Finding correlations between these would suggest that BELA and large-scale, neutral outflows are, in fact, associated. We judge those correlations to be significant for which the slope $(a \pm \delta a)$ satisfies $a > 3\delta a$ and for which Pearson's (parametric) and Spearman's (non-parametric) correlation coefficients each show a correlation at $\geq$90% confidence. Noting that there is one galaxy with high $\Delta v_{maxN}/\Delta v_{max}$ and FWHM/FW20 (F05024−1941) which could drive a correlation by itself, we require that the correlation exist with and without this galaxy present and that the slopes be consistent.

We find no significant correlations in the starburst galaxies alone (38 nuclei with [O III] data). When the Seyfert 2s are added (8 nuclei), correlations emerge between FWHM([O III]) and Δv_{maxN}, both in all the galaxies and in only those nuclei with BELA. Though the number statistics are low (7 − 8 nuclei), we also observe correlations between FWHM([O III]) and Δv_{maxN} in only the Seyferts with BELA. The fits to these data and correlation coefficients are listed in Table 7.

The observation of significant correlations between Δv_{maxN} and FWHM([O III]) may suggest a link between the neutral outflow and the NLR in Seyfert galaxies. The starburst galaxies alone do not exhibit these correlations; it appears that the presence of a Seyfert nucleus is necessary. Furthermore, there are no strong correlations between the high-velocity neutral and ionized gas (the latter is traced by FW20). Since FWHM([O III]) probes the outer part of the NLR ($r \lesssim 1$ kpc) in Seyferts, while the higher-velocity gas probably probes much nearer the nucleus (Veilleux 1991c), this may imply that the neutral gas in Seyferts is generally located in the 'extended' NLR of the galaxy.

A caveat is that the dynamics of the core of the [O III] line are strongly affected by the gravity of the bulge (Veilleux 1991b; Whittle 1992a,b; Nelson & Whittle 1996), and that the gas that contributes to the line emission is not purely outflowing. However, as Figure 5 demonstrates, when galaxies without BELA are removed, the scatter in the correlation decreases quite dramatically. This lends support to the idea that the blueshifted neutral and ionized gas are somehow linked, especially in Seyfert ULIRGs.

3.2.3. Individual Galaxies

The emission-line profiles in a few of these galaxies are worthy of individual mention. Note that we observe extended gas that is photoionized by the AGN in several galaxies.

Z03150−0219. This galaxy has a red emission-line component with velocities up to 800 km s^{-1} above systemic and a higher [O III] $\lambda 5007$/Hβ flux ratio than the gas at systemic by a large factor (≥ 10). No detectable Hβ emission is observed at this velocity.

F04210+0401. This galaxy possesses a large radio jet. We observed this galaxy with the spectroscopic slit aligned with the position angle of the jet, and observe spectacular emission-line structures that have been studied in previous works (e.g., Steffen, Holloway, & Pedlar 1996a,b). We observe a narrow and low signal-to-noise ratio Na I D component at systemic.

F05024−1941. This galaxy has the highest absorption-line velocity Δv of all starbursts and Seyfert 2s in our survey. A low-velocity blue wing is present, as well as an optically thick component with low covering fraction at $\Delta v = 1550$ km s^{-1}. This galaxy also has a redshifted absorbing component whose velocity is identical to that of an emission-line feature extending ~ 15 kpc to the south. The velocities of the [O III] line do not extend as far as $\Delta v = 1550$ km s^{-1}, but those of the [N II] $\lambda\lambda 6548, 6583$ line do. The peak of [O III] is blueshifted from systemic by ~ 470 km s^{-1}.

F05189−2524. This galaxy has numerous emission lines of various stages of ionization in its spectrum (superimposed on a continuum with deep stellar absorption lines; see also Farrah et al. 2005). The high-ionization lines (e.g., [O III], [Ar III] $\lambda\lambda$7137, 7752, and [S III] $\lambda\lambda$9069, 9531) are blueshifted by 510 km s^{-1} with respect to systemic (as determined by the stellar absorption lines and CO emission), while the low-ionization lines are at systemic. Some of the high-ionization lines also have blue wings extending even farther from systemic. The centroid of the blue component of Na I D is within 100 km s^{-1} of the peak of the high-ionization lines.

F08526+3720. There is extended emission $\sim$15 kpc to the north and south of this galaxy that has the same velocity as the outflowing Na I D; the high [O III]/Hβ flux ratio indicates this material may be ionized by the AGN.

F08559+1053. The peak of [O III] is located 200 km s^{-1} blueward of systemic, and [N II] has a blue component at this velocity. There is extended emission 5 kpc to the south of this galaxy at a velocity near systemic; this gas has [O III]/H$\beta \sim 5 - 6$, which implies ionization by the AGN. There are substantial variations between [O III]/Hβ in both position and velocity space, perhaps probing variations in density (i.e., substructure).

F13428+5608 (Mrk 273). This well-known Seyfert 2 shows extended line-emitting structures and complex velocity profiles on scales of up to $30 - 40$ kpc on both sides of the nucleus. Variations in Hα/[N II] are visible, including likely shock-excited regions several kpc to the NE and SW that also exhibit line-splitting of $300 - 400$ km s^{-1}. Larger line-splitting ($\sim$500 km s^{-1}) occurs at larger radii (see also Colina, Arribas, & Borne 1999).

4. OUTFLOWS IN SEYFERT 1 ULIRGS

4.1. Outflow Properties

In Figure 7, we display the Na I D lines in the 6 Seyfert 1 ULIRGs in our sample with our fits to the lines superimposed. Tables 2 and 3 list the measured properties of each Na I D velocity component and of the outflow in each galaxy, respectively. Table 4 lists the average outflow properties in this subsample.

We measure an outflow detection rate in Na I D of $\sim$50% (3 of 6 galaxies). On the surface, this is discrepant from the result of Boroson & Meyers (1992), who found blueshifted Na I D absorption lines in $3 - 4$ of 19 infrared-selected quasars and Seyfert 1s with warm infrared colors. However, if the galaxies in Boroson & Meyers (1992) are segregated by luminosity, the detection rate is 0% in non-ULIRGs and $40 - 60\%$ ($3 - 4$ of 7 galaxies) in

ULIRGs. Our detection rate is similar to that of intrinsic UV and X-ray absorbers in local Seyfert 1s ($50 - 70\%$; Crenshaw et al. 2003). It has interesting implications for the geometry of the Na I D absorbers in Seyfert 1s (§6.3) and for the relation of ULIRGs to low-ionization broad absorption-line quasars (§6.6.1).

The properties of the nuclear absorbers in these Seyfert 1 galaxies show clear differences from those found in Seyfert 2 and starburst galaxies, as we discuss below. They are thus powered by the AGN, rather than a starburst or starburst+AGN (§6.7). However, Seyfert 1s possess strong starbursts as well as AGN, and thus must contain an extended, starburst-driven outflow alongside a nuclear AGN outflow. The detection rate of extended outflows is 15%, since we observe them in only Mrk 231 (§5). Extended outflows are difficult to detect in Seyfert 1s due to the high luminosity of the nucleus.

Two galaxies (F07599+6508 and F12540+5708 [Mrk 231]) are broad-absorption-line quasars, and thus have very broad (FWHM $\gtrsim$ 2000 km s^{-1}) and deep absorption complexes with high maximum velocities (up to $\sim 10^4$ km s^{-1}). A third Seyfert 1 (F11119+3257) also possesses high-velocity, outflowing gas; the three components of the Na I D feature have central velocities of $\Delta v \sim 700 - 1400$ km s^{-1}. Velocities of this magnitude are found in one Seyfert 2 (F05024−1941) and one starburst (F10378+1108). However, the outflow properties in these two galaxies are different from those in F11119+3257 in that the covering fraction of the high-velocity gas is smaller ($C_f = 0.2 - 0.4$ vs. $0.7 - 1.0$ in F11119+3257), there is only a single high-velocity component (vs. three in F11119+3257), and there is low-velocity gas (there is none detected in F11119+3257). The properties of the absorbers in F11119+3257 are consistent with those of UV and X-ray intrinsic absorbers found in local AGN (§6.5; Crenshaw et al. 2003).

As we discuss below (§6.1), the nuclear absorption in Seyfert 1s is likely to arise on scales of tens of pc or less. In calculating the masses, momenta, and energies listed in Tables 1 and 4, we assume an absorbing radius of 10 pc. This yields masses, momenta, and energies of $10^{4.3}$ $M_\odot$, 10^{46} dyne s, and 10^{55} erg on average, values that are much smaller than those observed in Seyfert 2 and starburst galaxies. However, the outflow rates of these quantities are comparable to or larger than those in Seyfert 2s and starbursts due to the high observed velocities. On average, we compute $dM/dt = 12$ M$_\odot$ yr^{-1}, $dp/dt = 10^{36}$ dyne, and $dE/dt = 10^{44}$ erg s^{-1}. The energy outflow rate of the neutral gas is surprisingly large, at $\sim 1\%$ of the radiative luminosity of the galaxy on average.

4.2. Broad Absorption-Line Modeling

In Rupke, Veilleux, & Sanders (2002), we discuss in detail our method for modeling the broad absorption line (BAL) in Mrk 231. We have only slightly modified the results of this modeling for the current work. F07599+6508 is a more difficult case since, unlike Mrk 231, it has strong Fe II emission lines overlapping Na I D (e.g., Boroson & Meyers 1992) that are complex to model and remove. Rather than attempt to remove these lines, we have simply fit the continuum around the broad complex. This partially removes the emission feature that affects the blue half of the Na I D line (Boroson & Meyers 1992). However, we are insensitive to the very blueshifted absorption that Boroson & Meyers (1992) claim to see in this galaxy at $\sim$16000 km s^{-1} because of our decision not to model the Fe II lines.

The number of components that we should fit to each of the broad features is uncertain. In Mrk 231, we fit many narrow components to the broad profile. We use as a starting point the components suggested by Forster, Rich, & McCarthy (1995), who vary the number of components in the Na I D line and choose the number which gives the best fit. For F07599+6508, however, we fit only three very broad components to the deep Na I D feature; without doing a detailed analysis similar to that of Forster et al. (1995), it is unclear whether we should use few or many components. The conclusions of this paper are not sensitive to the details of the Na I D fits in the BAL Seyfert 1s, so we have chosen not to do more sophisticated modeling.

The Na I D absorption lines in F07599+6508 have been observed previously by other authors (e.g., Boroson & Meyers 1992). However, ours is the first attempt to model them using detailed profile fits. We note here that F07599+6508 also has BALs (both low- and high-ionization) in the UV with outflow velocities that range from $5000 - 22000$ km s^{-1} (Lanzetta, Turnshek, & Sandoval 1993; Lípari 1994; Hines & Wills 1995). These velocities are larger than those seen in Na I D ($4000-11000$ km s^{-1} in our spectra, or up to 16000 km s^{-1} in the spectra of Boroson & Meyers 1992). Furthermore, the broad Na I D absorption feature is not seen in polarized light (Hines & Wills 1995), suggesting that the global covering factor of the absorbing gas is less than unity (§6.3).

5. A CASE STUDY: SMALL- AND LARGE-SCALE OUTFLOWS IN MRK 231

5.1. Background

We observe an AGN-driven wind arising in the broad-line region of Mrk 231, a Seyfert 1. This conclusion is based on the observation of broad, high-velocity absorption lines in the nucleus, as well as on the time variability of the bluest component (§6.1). However, it was proposed by Hamilton & Keel (1987) that there is also a wide-angle, large-scale wind in this galaxy. They observe emission lines with blue asymmetries in a region that extends several kpc from the galaxy's nucleus in multiple directions. Line-splitting is also present in [O III] $\lambda 5007$ a few kpc to the south of the nucleus (at $v_\odot = 12100$ and 12600 km s^{-1}; Hamilton & Keel 1987) and in [O II] $\lambda 3727$ in the nuclear spectrum (at 11900 and 12700 km s^{-1}; Boksenberg et al. 1977). This implies blueshifts of $500 - 800$ km s^{-1} with respect to systemic (12642 km s^{-1}, from CO and H I data; Sanders, Scoville, & Soifer 1991; Carilli, Wrobel, & Ulvestad 1998).

These blueshifts and blue wings surrounding the nucleus are strongly suggestive of a large-scale outflow. However, given the ambiguous nature of emission-line kinematics in an interacting system where inflow could be present, it would be good to confirm this claim by looking for blueshifted absorption lines.

5.2. Present Observations

Mrk 231 is the closest galaxy (by a factor of 2.5) in our Seyfert 1 sample. We observed this galaxy in a short (5-minute!) exposure with ESI on Keck II. We later observed it again at Kitt Peak in a 4800 s exposure. The former instrument has a much better point-spread function (PSF) and spatial sampling, so we used this observation to decompose the near-nuclear profile. However, we note that the KPNO spectrum shows similar behavior. The long slit in the latter observation also reveals a faint emission-line region $10 - 17$ kpc south of the nucleus, which has a narrow linewidth of 135 km s^{-1}, is blueshifted from systemic by $150 - 200$ km s^{-1}, and corresponds to a stellar tidal feature or spiral arm in continuum and emission-line images (Hamilton & Keel 1987). (The velocity of this feature is misprinted in Hamilton & Keel 1987 as being 700 km s^{-1} *above* systemic.)

Along the north-south slit, we extracted thirteen, $0\!\!''\!8$-wide regions and fit the Na I D feature in each one. We detect low-velocity blueshifted Na I D absorption lines ($\Delta v \gtrsim -2100$ km s^{-1}) in most of these spectra, over a projected extent of 6 kpc. In Figure 8, we

plot the spectrum of each region in which we fit the low-velocity absorption. This absorption arises in the nuclear spectrum, but the lines are difficult to see here because they have low equivalent width and arise at the juncture of what may be overlapping broad emission lines (He I $\lambda5876$ and Na I D). In the two northernmost spectra we did not detect low-velocity Na I D to the limit of our signal-to-noise ratio. From these spectra, we see that the velocities and profiles of the absorbers vary significantly across the disk, and are rather clumpy in the northern regions. We also see that the gas has much higher velocities north of the nucleus than south of the nucleus.

As further illustration, in Figure 9 we plot, as a function of slit position, the velocities of (a) the low-velocity Na I D components; (b) the narrow components of Hα and [S II] $\lambda\lambda6716$, 6731; and (c) the Ca II triplet (where available). Along the north-south slit, the stellar absorption-line and gaseous narrow-line velocities are consistent with the systemic velocity of the nuclear disk (to within ±50 km s^{-1}). In the 8 extra-nuclear bins where we fit the low-velocity Na I D line, the blueshifted interstellar gas reaches a velocity of at least 300 km s^{-1} with respect to systemic (and up to 2100 km s^{-1} in one bin).

The nuclear spectrum spills into the spectra of the extended regions due to the wings of the PSF. We confirmed that the newly-discovered, low-velocity absorption is not an artifact of PSF smearing by computing the ratio of the equivalent width of the broad, high-velocity component to that of the low-velocity component. This ratio decreases dramatically away from the three nuclear bins (by a factor >100), meaning that the low-velocity absorption occurs over an extended region.

We detect two extended continuum components besides the nuclear component; these serve as the background illumination for the extended absorbers. There is an extended baseline component, as well as a peak in continuum flux $3 - 4''$ south of the nucleus. A bright emission-line region with a LINER spectrum is also present near the southern peak, offset slightly towards the nucleus. In general, the extranuclear regions of Mrk 231 contain numerous blue star-forming knots with a range of ages ($\sim10^7 - 10^9$ yr). These knots are especially dense in the southern region in which we detect a second continuum peak and emission-line spectrum, the 'horseshoe' region of Hamilton & Keel (1987).

We observe redshifted emission in Na I D in the spectrum 2.3 kpc north of the nucleus (see Figure 8). This is not light contamination from the nuclear spectrum, since the emission is not broad and there is no emission in the southern spectra at the same distance from the nucleus. The observed redshifted velocities match the lower range of blueshifted velocities; this emission may be resonant scattering from receding gas.

We also observe the blueshifted emission-line wings in [N II] $\lambda\lambda6548$, 6583 claimed by

Hamilton & Keel (1987). There is some uncertainty in this result due to telluric absorption of the [N II] $\lambda6583$ line and to broad Hα from the nuclear spectrum that contaminates the near-nuclear bins. Farther from the nucleus, the conclusion is more secure. The velocities appear greater than or equal to those in absorption, as seen in other objects.

Finally, there is clear evidence of line-splitting in Hα and [N II] in the two northernmost bins, with blue- and red-shifted velocities of $100 - 200$ km s^{-1}. The emission lines present a higher [N II]/Hα flux ratio $(1.1 - 1.2)$ than elsewhere, suggesting the presence of shock ionization. Accompanying the line-splitting, there is a faint blueshifted emission-line component in these spectra with velocity relative to systemic of ~800 km s^{-1} (or larger, if it is not [N II] $\lambda6548$). There is a probable redshifted counterpart of similar velocity redward of [N II] $\lambda6583$. A high-velocity blueshifted component is also seen south of the nucleus by Hamilton & Keel (1987).

5.3. Interpretation

What is the explanation for the gas dynamics in this source? The blueshifted absorption lines point to an extended outflow. Consistent with this scenario are the observed blue emission-line wings, line splitting, high-velocity emission-line components, and redshifted Na I D emission. The presence of comparable-velocity blue- and redshifted components in absorption and emission could arise on the approaching and receding sides of a spherical or biconical outflow. The best interpretation is that of a large-scale, wide-angle wind.

The difference in north and south absorption-line velocities argues against a model for the wind where the absorption arises on the surface of the wind; in this model, the outflow velocity should be the same at a given radius north or south of the nucleus. If we assume instead that the absorption arises in the walls of the outflow in the side of the outflow facing our line-of-sight, then the variations can be attributed to projection effects. Consider a model of a constant-velocity, bipolar, wide-angle wind emerging perpendicular to the H I/CO disk. We can calculate the expected inclination of the disk and opening angle of the outflow from the ratio of the observed maximum velocities north and south of the nucleus. A reasonable range for this ratio is $v_{south}/v_{north} \sim 0.2 - 0.4$, using the maximum observed values of $v_{north} = 1000 - 2000$ km s^{-1} and $v_{south} = 400$ km s^{-1}. The resulting calculated disk inclinations $(i = 25 - 40°)$ are consistent with those observed (Bryant & Scoville 1996; Carilli et al. 1998), and the resulting wind opening angles $(65 - 90°)$ are consistent with those expected based on observations of local starburst and Seyfert 2 outflows (Colbert et al. 1996a; Veilleux et al. 2005).

Because Mrk 231 has both a strong starburst and a strong AGN, the power source of this wind is ambiguous. The maximum outflow velocity is larger than in any starburst or Seyfert 2 galaxy we observe. If the wind is AGN-powered, the power could come from a wide-angle wind originating at scales of a few to tens of parsec, or could result from a jet dumping energy into the ISM of the host galaxy. In 3C 305, neutral gas with comparable velocities and on similar spatial scales to the outflow in Mrk 231 arises as the radio jet interacts with the ISM (Morganti et al. 2005).

In fact, there is a north-south radio jet in this galaxy on scales ranging from tens of pc to tens of kpc (Carilli et al. 1998; Ulvestad, Wrobel, & Carilli 1999). This jet is probably perpendicular to the kiloparsec gas disk seen in CO (Bryant & Scoville 1996; Downes & Solomon 1998), H I (Carilli et al. 1998), and radio continuum emission (Carilli et al. 1998; Taylor et al. 1999). The disk has an inclination of $\lesssim 60°$ (Bryant & Scoville 1996), perhaps close to 45° (Carilli et al. 1998), with respect to the plane of the sky and a roughly east-west major axis position angle. (However, Downes & Solomon 1998 argue for $i \lesssim 20°$.) The northern half of the disk appears to be the near side (Carilli et al. 1998), meaning that the jet is approaching from the south and receding to the north. This is inconsistent with the higher velocities observed north of the nucleus than south of the nucleus, suggesting that the gas dynamics we observe are not directly connected with the jet's motion.

6.   DISCUSSION

6.1.   Location of Absorbing Gas

Our absorption-line data contain limited information about the galactocentric radius at which the absorption occurs. A typical method in absorption-line studies is to use photoionization codes to determine the radius. Since we have information on only one transition in a single atomic species, this technique is unavailable to us. However, by using simple physical arguments and comparing to other data we can make some useful statements.

6.1.1.   Seyfert 1s

There are several physical arguments that we can make that the broad absorption lines observed in F07599+6508 and Mrk 231 arise at small scales. First, the high velocities observed ($\Delta v \sim 10^4$ km s^{-1}) are comparable to emission-line velocities observed in the broad-line region, which extends ~ 0.1 pc from the black hole. Second, the bluest component in the nucleus of Mrk 231 is time-variable in both velocity and equivalent width (Boroson

et al. 1991; Forster et al. 1995; Rupke et al. 2002; Gallagher et al. 2005). Variability on short timescales can imply short distances to the ionizing source (Crenshaw et al. 2003). Third, the mass and energy outflow rates from these nuclei are too large if we assume $r = 1$ kpc. For F07599+6508 and Mrk 231, this yields mass outflow rates of several thousand $M_\odot$ yr^{-1}. This will move over 10^{10} $M_\odot$ of gas in only 10 million years, which is a substantial disruption. If these winds are driven by black hole accretion, these mass outflow rates are at least 1000 times the Eddington accretion rate for a mass-to-energy conversion efficiency of 0.1 and a bolometric luminosity of 10^{46} erg s^{-1} (as in Mrk 231). Finally, the whole luminosity of the galaxy would be driving the outflow, since the energy outflow rate (10^{46-47} erg s^{-1}) would be comparable to the galaxy's luminosity!

These arguments do not apply to F11119+3257, whose outflow velocity is much smaller ($\lesssim 1500$ km s^{-1}). Indirect evidence, including comparisons with other galaxies in our sample (§4.1) and with UV and X-ray intrinsic absorbers in Seyfert 1s (§6.5), suggests that the absorbers are at small radius (i.e., tens of pc or less).

We conclude that the nuclear Na I D absorbers in our Seyfert 1 subsample almost certainly arise on small scales. In calculating the masses, momenta, and energies listed in Tables 1 and 4, we therefore assume an absorbing radius of 10 pc (i.e., in the inner NLR). However, we cannot *rule out* absorbers on larger scales in the nuclear spectra of these galaxies, since there are isolated cases of broad absorbers (de Kool et al. 2001) and narrow absorbers (Hamann et al. 2001) arising on scales of hundreds of pc to tens of kpc. In fact, larger scale outflows (powered either by a starburst or the AGN) probably occur in most of these galaxies, as in Mrk 231, but we cannot detect them due to limitations in spatial resolution and nuclear contamination.

6.1.2. Seyfert 2s

The absorbers in Seyfert 2s have different properties than those in Seyfert 1s. They are similar to the absorbers in starbursts, which lie at kpc radii (Paper II).

We directly observe extended, blueshifted absorption in three Seyfert 2s (F05189−2524, F13451+1232, and F15001+1433). This absorption arises several kpc from the nucleus in F05189−2524 and up to radii of $10-15$ kpc in the other two galaxies. For F05189−2524, two other lines of evidence suggest large-scale outflow. A low-resolution spectrum, obtained with the Space Telescope Imaging Spectrograph (STIS) on *HST*, probes nuclear radii of $\lesssim 200$ pc (Farrah et al. 2005). This spectrum does not show the deep Na I D absorption observed in our ground-based data; we measure equivalent widths of 0.7 Å and 5.4 Å for the *HST*

and ground-based spectra, respectively. This implies that the strong, blueshifted absorption occurs primarily at a projected radius of $\gtrsim 200$ pc. Furthermore, the background source is not the core of the Seyfert nucleus, but rather a more extended continuum source (a result that is consistent with the strong stellar lines observed in the ground-based spectrum). In our ground-based spectrum, we also observe redshifted Na I D *in emission* at a distance of ~ 2 kpc from the nucleus. Similar behavior is seen in the outflow in NGC 1808; this emission is interpreted as resonance scattering by the receding part of the outflow (Phillips 1993). The velocity of this emission is consistent with this interpretation, as it appears to be redshifted roughly 100 km s^{-1} from systemic (matching the velocity of the blueshifted absorbing component nearest to systemic). Another potential origin of this emission is scattered light from the broad line region of the nucleus, but we do not observe this signature in other emission lines in this object in the offset spectra.

Indirect evidence for kpc outflows in Seyfert 2s comes from emission/absorption line correlations. If the Na I D outflow were located in the inner NLR ($r \lesssim 100$ pc), one might expect a correlation of high-velocity ionized gas (as parameterized by the full-width at 20% maximum of the [O III] $\lambda 5007$ line) with the maximum outflow velocity of the neutral gas (Δv_{max}). We do not observe such a correlation (§3.2.2). Instead, we observe a correlation between the width of the core of the [O III] $\lambda 5007$ line and the lower-velocity neutral gas, which is natural in the case of a wind arising in the 'extended' NLR ($r \gtrsim 0.1 - 1$ kpc).

6.2. Dependence of Outflow Properties on Galaxy Mass and Luminosity

In Paper II, we studied outflow properties as a function of galaxy properties in our sample of 78 infrared-luminous starbursts. We also included Na I D observations of four dwarf starbursts (Schwartz & Martin 2004). We found an increase in outflow velocity, mass, momentum, and energy as a galaxy's star formation rate, luminosity, and circular velocity (mass) increase. The increases in outflow velocity, mass, etc. with SFR are natural in a model where the ram pressure of supernova-heated gas drives ambient material out of the starburst. Radiation pressure probably also plays a role, given the high luminosity and dustiness of many of these galaxies. However, its momentum input at a given infrared luminosity is an order of magnitude less than that from star formation. Thus, supernovae-heated gas is *necessary* to power the outflows observed in many objects.

In Paper II, we also showed that these trends of outflow properties with galaxy properties become shallow or disappear at high values of SFR, luminosity, and v_c (i.e., in the ULIRG population). We cannot conclusively demonstrate why this is so, though there are several possible explanations: (a) the entrainment of all available gas clouds; (b) a velocity threshold

due to the finite velocity of the hot wind (Murray, Quartaert, & Thompson 2005; Martin 2005); or (c) a reduction in thermalization efficiency at high SFR, luminosity, and v_c.

Our sample of Seyferts is too small to look for correlations, but we can compare the phase-space locations of our Seyfert galaxies with those of the starbursts. In Figures $10 - 13$, we plot maximum velocity, mass outflow rate, momentum outflow rate, and energy outflow rate vs. infrared luminosity and circular velocity.

All of the Seyfert 2 points fall in the regions of these plots populated by starburst ULIRGs. This similarity reinforces the idea that the outflows in Seyfert 2 and starburst ULIRGs are largely similar (see also §3 and §6.7). Furthermore, the momentum and energy injected from the starburst are sufficient to explain the momentum and energy in the outflows in Seyfert 2 ULIRGs, implying that the contribution from the AGN is comparable to or smaller than that from the starburst. Finally, Figure 13 again illustrates the point that, on average, Seyfert 2s and starbursts have approximately the same mechanical luminosity per unit radiative luminosity (see §3.1).

6.3. Frequency of Occurrence and Global Covering Factor

As we discuss in Paper II, the detection rate D is a function of both the actual frequency of occurrence of winds F and the global angular covering factor of the wind, Ω. The global angular covering factor, or solid angle subtended by the wind, is the product of the large-scale opening angle (given by C_Ω, a fraction of 4π) and local clumping (which we assume to be represented by C_f). The opening angle is given by the detection rate if the frequency of occurrence of winds is 100%, as in starbursts. The global covering factor is thus $\Omega/4\pi = C_\Omega \langle C_f \rangle = D \langle C_f \rangle$ (Paper II; see also Crenshaw et al. 2003). In the more general case, we can set lower limits to F and C_Ω using our detection rate: $D < F \leq < 1$ and $D < C_\Omega \leq 1$.

Assuming $F = 1$ for Seyfert 2s (as in starbursts of comparable SFR; Paper II), we measure $C_\Omega = D = 0.45 \pm 0.1$. This corresponds to wind opening angles of $100 - 125°$, consistent with measurements of winds in local Seyfert 2s (e.g., Colbert et al. 1996a; Veilleux et al. 2005). If instead we assume $F = D = 0.45$, then the projected wind opening angles of 360° are inconsistent with measurements. We thus conclude that winds occur in most Seyfert 2s. Using the value of $\langle C_f \rangle$ listed in Table 4, we compute that the average global covering factor of neutral gas in these winds is $\Omega/4\pi = 0.19$, close to the value measured in IRGs (Paper II).

For Seyfert 1s, the detection rate of Na I D absorbers (both broad and narrow) is $\sim$50% (based on this work and Boroson & Meyers 1992), and the average C_f is 0.7 (Table 4).

Assuming $F = 1$ for Seyfert 1s, we compute $D = 0.5 \pm 0.1$ and $\Omega/4\pi = 0.4$. This result is consistent with the value of $\Omega \sim 0.5$ measured from observations of intrinsic, narrow, high-ionization absorption lines in local Seyfert 1s (Crenshaw et al. 2003). It is also consistent with the lack of observed broad Na I D in polarized light in F07599+6508 (Hines & Wills 1995), from which we can infer that the global covering factor of Na I D absorbers in Seyfert 1 ULIRGs is not generically of order unity.

6.4. Gas Escape Fraction

There are several Seyfert 2 galaxies with very high velocities in our sample. This means that some of this material, if it is at large enough radius and does not encounter substantial drag from interstellar gas, will escape the galaxy and enter the intergalactic medium. It is difficult to estimate precise escape velocities for these galaxies. However, we can make simplifying assumptions that allow us to calculate an 'escape fraction' of gas. We consider this illustrative rather than strictly quantitative due to the uncertainties.

As in Paper II, we assume a singular isothermal, spherical density distribution with a density that truncates at a radius r_{max}. If the gas absorbs at radius r, then the escape velocity is parameterized uniquely by v_c and r_{max}/r. Our procedure to calculate f_{esc} is as follows: (a) to get v_c, use measured values where possible; otherwise, use an average from measurements of other ULIRGs (K. Dasyra, private communication); (b) use v_c to compute v_{esc}; (c) compute the mass outflow rate of gas that has a velocity above v_{esc}; (d) sum dM/dt and dM/dt_{esc} over all galaxies with measured v_c; and (e) divide dM/dt_{esc}^{total} by dM/dt^{total}. (Note that M and dM/dt are interchangeable in this algorithm; the values of f_{esc} computed using M are comparable to those computed using dM/dt, but smaller by a factor of 2. The discrepancy is due to the extra factor of Δv in the definition of dM/dt; see Paper II.)

Using this procedure, we measure $f_{esc} \lesssim 60\%$ for the neutral outflowing gas in AGN-dominated ULIRGs, which is much higher then the value of $\lesssim 20\%$ measured for starbursts. Thus, the neutral, dusty outflowing gas in these galaxies may play a significant role in enriching the intergalactic medium at higher redshifts, where the number density of ULIRGs is high. Furthermore, the hot free wind that drives the expansion of the large-scale winds in starbursts may also be present in these systems. This gas is metal-enriched and has more specific energy than the neutral phase. It is hence more likely to escape the galaxy and enter the IGM.

6.5. Connection to Intrinsic Absorbers in Seyfert 1s

It is instructive to compare our results to those found in UV and X-ray absorption-line studies of local ($z < 0.1$), moderate-luminosity ($\log[L_{\rm bol}/L_\odot] \sim 10 - 12$) Seyfert 1s. The observed intrinsic (or 'warm' in the X-ray case) absorbers in these galaxies probably arise on scales of tens of pc or smaller and are thus powered by the AGN (e.g., Crenshaw et al. 2003; Crenshaw & Kraemer 2005; McKernan et al. 2005).

Similarities in detection rate, column density, and velocity exist between the absorbers we detect in Seyfert ULIRGs and intrinsic absorbers. The detection rate of intrinsic absorbers in Seyfert 1s is $50 - 70\%$ (Crenshaw et al. 2003). Measured UV and X-ray column densities of some absorbers (Crenshaw et al. 2003; McKernan et al. 2005) are also consistent with our measurements of $N(\rm H) \sim 10^{21-22}$ cm^{-2}. Finally, the distribution of velocities in intrinsic absorbers (ranging up to 2300 km s^{-1}; Crenshaw & Kraemer 2005; McKernan et al. 2005) is broadly consistent with what we measure in Na I D in Seyfert 2s (Figure 2) and in one Seyfert 1, F11119+3257. In the UV, the majority of observed components (75%) have $\Delta v > -700$ km s^{-1}, and there are some redshifted components with velocities up to 200 km s^{-1} (Crenshaw & Kraemer 2005). Out of 14 X-ray 'warm absorbers' modeled in McKernan et al. (2005), 10 have velocities less than 1000 km s^{-1}, though there are no redshifted components.

However, the distribution of FWHM in UV absorbers is not consistent with our measurements. Most of UV absorbers (80%) have FHWM < 100 km s^{-1} (Crenshaw & Kraemer 2005), while the average Na I D FWHM in Seyfert 2 ULIRGs is 400 km s^{-1} (Table 4 and Figure 2). In the X-ray the situation is less clear, as most components are unresolved (FWHM $\lesssim 200 - 300$ km s^{-1}; McKernan et al. 2005).

This difference, as well as the conclusion that Na I D absorbers in Seyfert 2s are located at galactocentric radii of $r \gtrsim 1$ kpc (§6.1), suggest that the neutral absorbers are not directly related to Seyfert 1 intrinsic absorbers. However, the lines we observe in F11119+3257 could be an optical manifestation of intrinsic absorbers. The Na I D components in this galaxy are high in velocity and covering fraction and low in velocity width (§4.1 and Table 2).

6.6. Outflows and Merger Evolution

Most ULIRGs are in the late phase of a merger between two massive, gas-rich galaxies (Veilleux et al. 2002). We showed in Paper II that the detection rate of outflows in ULIRGs does not obviously depend on merger phase. There is some variation of outflow velocity with interaction class, but our sample size is too small to show that this is significant. Adding the Seyfert 2s to the starburst sample does not change the conclusions of Paper II in this

regard.

Seyfert ULIRGs are on average later in the stages of merging than starburst-dominated ULIRGs (Veilleux et al. 2002). We now discuss our observations in light of the mechanisms by which they may be removing the obscuring dust screen surrounding the AGN and evolving into optical quasars or radio galaxies.

6.6.1. ULIRG Connection to Broad Absorption-Line Quasars

Orientation-based models and evolutionary models compete to describe the properties of broad absorption lines (BALs) found in quasars. The latter are meaningful in the context of ULIRGs, as BAL outflows could be a mechanism for removing the screen of dust surrounding ULIRG nuclei, converting them from obscured AGN to bright quasars.

Out of ten Seyfert 1 ULIRGs observed by us and Boroson & Meyers (1992), at least four are low-ionization BAL quasars (loBALQSOs; Weymann et al. 1991; Boroson & Meyers 1992). Two or three of these ten possess BALs in Na I D (F07599+6508, Mrk 231, and possibly F17002+5153), and two others possess narrow Na I D absorption (F11119+3257 and F14026+4341). LoBALQSOs are more common in IR-selected than optically-selected quasar samples (27% vs. 1.4%; Boroson & Meyers 1992). As we show, they are apparently even more common in ULIRG samples, with a detection rate of $\geq (40 \pm 10)\%$.

The loBALQSOs as a class have a number of unique properties. These include weak [O III] $\lambda5007$ (Boroson & Meyers 1992), strong Fe II lines (Weymann et al. 1991), red continua (Weymann et al. 1991), and relatively weak X-ray flux and/or high absorbing columns (Gallagher et al. 2001). It has been hypothesized that loBALQSOs have high global covering factors, and that IR-luminous loBALQSOs may represent a stage in the life of quasar when the nucleus is enshrouded in dust and is in the process of destroying this screen via fast outflows. Thus, loBALQSOs may be an evolutionary stage in the proposed scenario by which some quasars are formed from major mergers. In this scenario dust-enshrouded ULIRGs are an intermediate stage between the merger and a quasar. This scenario does not conflict with recent sub-mm observations showing that BALQSOs and QSOs have similar dust properties (Willott, Rawlings, & Grimes 2003), since most of the BALQSOs observed were not loBALQSOs. The merger-to-loBALQSO-to-QSO model is also consistent with our measurement of the global covering factor of Na I D-absorbing gas in Seyfert 1 ULIRGs ($C_\Omega \sim 0.4$).

6.6.2. ULIRG Connection to Radio Galaxies

Galaxies may also undergo a radio-loud stage in the evolution from a merger remnant to an unobscured QSO. Young, massive, and reddened stellar populations (ages $0.1-1$ Gyr) are observed in a number of radio galaxies on kpc scales (e.g., Tadhunter et al. 2005). The radio jets in these galaxies could be triggered by a massive merger that funnels gas to the nucleus and feeds the central black hole; given the observed stellar ages, the jet turns on late in the merger sequence (Tadhunter et al. 2005). In a number of radio galaxies, a jet interacts with the surrounding ISM at kpc or sub-kpc radii and powers massive $[N(\mathrm{H}) = 10^{21-22}\ \mathrm{cm}^{-2}]$, high-velocity ($\Delta v \lesssim 2000$ km s^{-1}) outflows of neutral and ionized gas (Morganti et al. 2003 [3C 293]; Morganti et al. 2004b; Holt, Tadhunter, & Morganti 2003 [4C 12.50]; Morganti et al. 2005 [3C 305]; Morganti et al. 2001 [PKS 1814-63 and 3C 459]). This phenomenon is also observed in at least one Seyfert 2 galaxy with a radio jet, IC 5063 (Morganti et al. 1998; Osterloo et al. 2000; Morganti et al. 2004a).

These high-velocity outflows, observed in H I 21 cm and optical emission lines, could have counterparts in our data. In general, comparing our data to broad-band H I absorption observations is a good way to confirm our column density measurements; radio-loud galaxies are the easiest sources in which to do this comparison, since they provide a bright background continuum source.

Seven objects in our sample have 1.4 GHz fluxes >100 mJy, based on FIRST (Becker, White, & Helfand 1995) or NVSS (Condon et al. 1998) fluxes. There has been no systematic search for radio jets in these seven galaxies, but three are known to possess radio jets: F12265+0219 (3C 273), Mrk 231, and F13451+1232:W (4C 12.50). Two others may possess small-scale, low-power jets – F13428+5608 (Mrk 273; Carilli & Taylor 2000; Klöckner & Baan 2004) and F23389+0300:N (Nagar et al. 2003). The two other galaxies with f(1.4 GHz) >100 mJy and without known jets are F11119+3257 and F17179+5444. An eighth galaxy with a lower radio flux (F04210+0401) also possesses a radio jet. Out of these eight galaxies with high radio fluxes and/or jets, we observe outflows in Na I D in 4 objects, and in 3 of the 6 galaxies with known jets (see Table 3).

4C 12.50 is interesting because it is the one Seyfert 2 galaxy in our sample with both a powerful, extended radio jet and a Na I D outflow. This galaxy has single-dish and very-long baseline interferometer (VLBI) H I observations (Morganti et al. 2004b) and previous long-slit optical observations (Holt et al. 2003) with which to compare our data. The H I component seen in the western nucleus with VLBI (Morganti et al. 2004b) and the average optical emission-line peak redshift agree to within a few tens of km s^{-1}. This suggests that the high-velocity blue wings in the recombination and forbidden lines (Holt et al. 2003) are in fact high-velocity outflowing gas. We measure the peaks of these emission lines along a

PA of 104° (the line connecting the two nuclei), and our results are in quantitative agreement with those of Holt et al. (2003).

In our analysis (§2.5), we extracted the light in this galaxy using two apertures, one for each nucleus, yielding a $\Delta v_{max} = 360 \mathrm{km\ s^{-1}}$ outflow in the eastern nucleus. An extraction with more apertures confirms this picture. There is gas blueshifted by $\lesssim 400 - 500$ km s^{-1} from the emission-line peaks over a region extending at least 10 kpc eastward of the eastern nucleus. These velocities do not reach those of the high-velocity H I gas ($|\Delta v| = 700 - 1100$ km s^{-1}; Morganti et al. 2004b) seen in single-dish data, so it is unclear whether they are related. Our data, however, were not taken along the PA of the radio jet, which is 160° on scales of $\sim$100 pc (Stanghellini et al. 1997). There is no clear link between the jet and either the H I outflow (Morganti et al. 2004a) or the Na I D outflow; further observations are needed.

The Seyfert 1 Mrk 231 also possesses a radio jet on scales of tens of pc to tens of kpc (see §5). This galaxy has neutral and ionized gas outflows on kpc scales at velocities up to $\sim$2100 km s^{-1}, along the same axis as the radio jet. Thus, Mrk 231 may be a ULIRG analogue to the radio galaxies with young stellar populations that are experiencing high-velocity outflow seen in H I, and could serve as an evolutionary link between the two. It could represent a stage where the radio jet and corresponding neutral gas outflow have recently removed the dust screen from the galaxy's active nucleus. Low-resolution *Very Large Array* observations of the nucleus at the velocities of the BALs have not revealed any H I absorption in Mrk 231 (Carilli et al. 1998), but sensitive, broad-band, single-dish H I data just blueward of systemic do not exist for this galaxy (i.e., to study the extended absorbing gas).

Clearly, a sensitive broad-band search for H I absorption in radio-loud Seyfert ULIRGs is in order to better study the connection between Na I D outflows in ULIRGs and H I outflows in radio galaxies, as well as the implications for the evolutionary link between mergers, radio galaxies, and quasars. Mrk 231 would be an excellent target to begin this search.

6.7. Starburst- or AGN-Powered Winds?

Is there evidence from our data that AGN help to power large-scale, wide-angle outflows in Seyfert 1 and 2 ULIRGs? The fact that the infrared luminosities of many of these galaxies may be dominated by (dust-reprocessed) radiation from an AGN rather than a starburst does not a priori imply that the outflows we observe in Na I D are AGN-driven. The star formation rates in these galaxies are still high ($\gtrsim$100 M$_\odot$ yr^{-1}), and thus a starburst should be able to

power an outflow on its own.

6.7.1. Seyfert 1s

The broad absorption lines we observe in two Seyfert 1 galaxies (F07599+6508 and Mrk 231) are unique, as these types of profiles are not found in pure starbursts and belong to the class of BALs found only in quasars. These lines are most likely produced in or near the broad-line region of the AGN (§6.1). The properties of the narrow, low-velocity ($|\Delta v| \lesssim 1450$ km s^{-1}) lines in F11119+3257 are similar to UV and X-ray intrinsic absorbers in local Seyfert 1s and different from absorbers in starburst ULIRGs (§§4.1 and 6.5). They are thus probably powered by the AGN, as well.

The large-scale outflow components in Mrk 231 may be either starburst- or AGN-driven. The high velocities observed ($\Delta v \lesssim 2100$ km s^{-1}) and the presence of a strong jet suggest that the AGN may play some role, though there is certainly a starburst contribution, as well.

In short, the dominant contribution to Na I D absorbers in nuclear spectra of Seyfert 1s is from the AGN; on larger scales, both the AGN and a nuclear starburst may play a role. As we show for Seyfert 2s, disentangling the contribution of the two on these scales is difficult.

6.7.2. Seyfert 2s

We have shown above that the properties of outflows in Seyfert 2s are statistically consistent with those in starburst galaxies (§3.1). There is a hint of AGN contribution to the wind in the higher velocities observed, but this is not conclusive. The two-dimensional phase-space distributions of starbursts and Seyfert 2s relating outflow and galaxy properties are essentially indistinguishable, as well (§6.2). Thus, the effect of AGN on outflows in Seyfert 2s is difficult to ascertain; more observations are required. Certainly we can say that the momentum and energy contribution to the large-scale outflow from the AGN is comparable to or smaller than the energy contribution from the circumnuclear starburst also present in Seyfert 2 ULIRGs. (We assume that there are already powerful starburst-driven winds in these galaxies, as expected based on their star formation rates and the results of Paper II). Furthermore, the outflow mechanical energy per unit luminosity in IR-selected starbursts and Seyfert 2 ULIRGs is the same on average.

Two arguments provide some evidence for energy injection into the wind from an AGN. (1) The outflow detection rate and median star formation rate are similar in Seyfert 2 ULIRGs and the starburst IRGs, but their outflow velocity distributions are significantly

different (§3.1). (2) The correlation between the low-velocity neutral gas and the FWHM of [O III] $\lambda 5007$ (§3.2) is driven by the Seyfert 2 galaxies in our sample, indicating a connection between the neutral outflow and the extended NLR.

7. SUMMARY

We have demonstrated that outflows are a common phenomenon in infrared-selected galaxies, both in starbursts (Papers I and II) and Seyferts (this work). Here, we summarize our conclusions about outflows in infrared-luminous Seyferts.

(1) **Detection Rate.** We find a $\sim 45\%$ detection rate in infrared-luminous galaxies (mostly ULIRGs) that are optically classified as Seyfert 2s. This detection rate is lower than in starburst ULIRGs, but comparable to that in lower-luminosity starbursts. We argue that the detection rate reflects the wind geometry, and that outflows are found in all Seyfert 2 ULIRGs. Given that Seyfert 2 ULIRGs host strong starbursts, and that all infrared-luminous starbursts host large-scale outflows (Paper II), this is expected.

The presence of strong starbursts in Seyfert 1s implies that extended outflows also exist in the majority of these galaxies, but the high luminosities of the nuclei prevent their detection (except in Mrk 231). The Na I D outflow detection rate in the nuclear spectra of Seyfert 1 ULIRGs is still high ($\sim 50\%$), but these nuclear outflows are physically distinct from those in Seyfert 2s and starbursts.

(2) **Velocities.** We measure typical outflow velocities and maximum velocities of -220 and -450 km s^{-1}, respectively, in Seyfert 2 ULIRGs. The upper limit for $|\Delta v_{max}|$ is high, however, at 1550 km s^{-1} (in F05024$-$1941). There are few statistically significant differences between the velocities of Seyfert 2 ULIRGs and starbursts of comparable luminosity. However, some significant differences arise when comparing Seyfert 2s to starbursts of lower infrared luminosity. When separating our entire sample by spectral type, Seyfert 2s and LINERs have no significant differences in velocity, while H II galaxies differ significantly from both LINERs and Seyfert 2s.

We find very high (up to $\Delta v \sim 10^4$ km s^{-1}) velocities in two broad absorption-line (BAL) Seyfert 1s. The velocities in the nuclear spectrum of one Seyfert 1, F11119+3257, are lower, however; these absorbers may be analogous to UV and X-ray intrinsic absorbers in local Seyfert 1s. We also find extended, high-velocity ($\Delta v \lesssim 2100$ km s^{-1}) absorption in Mrk 231, confirming a suggestion by Hamilton & Keel (1987) that this galaxy hosts a large-scale outflow along with its nuclear BAL outflow.

We observe significant correlations between the velocity of the highest column density neutral gas and the FWHM of the [O III] $\lambda5007$ line in the combined starburst + Seyfert 2 sample. This implies that the ionized and neutral gas are physically connected and could indicate a connection of neutral outflows to the narrow-line region in Seyferts. However, the highest-velocity ionized and neutral gas are not significantly correlated.

(3) Radius. The nuclear absorbers in the two BAL Seyfert 1s in our sample and in F11119+3257 probably arise on scales of tens of parsec or less. However, we also observe blueshifted absorption at scales up to 4 kpc from the nucleus of Mrk 231. In Seyfert 2s, the absorbing gas likely arises on kpc scales. We directly observe extended, blueshifted absorption in three Seyfert 2s, and other lines of evidence support this picture.

(4) Starburst or AGN? The lack of statistically significant differences between outflows in Seyfert 2 ULIRGs and those in starburst ULIRGs implies that the contribution of the AGN to the large-scale outflows in these galaxies is comparable to or less than the contribution of the starburst. (This assumes that there are starburst-driven winds in these galaxies, a conclusion based on the high star formation rates of Seyfert 2s and the results of Paper II.) Furthermore, we find that the outflow mechanical luminosity per unit radiative luminosity is the same for Seyfert 2s and starbursts (5×10^{-4} on average).

Evidence for some AGN contribution to the wind comes from the observation that there are significant differences between the velocities of outflows in Seyfert 2 ULIRGs and starburst IRGs, while their outflow detection rates and star formation rates are similar. The correlation between low-velocity neutral and ionized gas also suggests a connection of the outflow to the extended NLR.

The outflowing Na I D absorbers we observe in Seyfert 1s are powered dominantly by the central black hole engine and emerge on small scales. This is based on physical arguments and comparison to the properties of intrinsic absorbers. There are most likely starburst- or AGN-powered outflows in the host galaxies of most Seyfert 1s, as well, as illustrated by Mrk 231. The high nuclear luminosity limits detection of a large-scale outflow in other galaxies.

(5) Context. ULIRGs are believed to be part of an evolutionary sequence in which two massive, gas-rich galaxies merge; a dusty, intense starburst is created; the obscuring dust is blown away to reveal a quasar; and the galaxy evolves into an elliptical (e.g., Sanders et al. 1988). The small- and large-scale starburst- and AGN-driven outflows that we observe in these galaxies may be a part of this process. Several of the Seyfert galaxies in our sample reveal unique stages in this process. Particularly, the Seyfert 1s that show low-ionization BALs may be instances where dusty material near the quasar is being blown away. Two

of the Seyfert galaxies in our sample (Mrk 231 and 4C 12.50) also host strong radio jets and outflows in Na I D. The latter contains a high-velocity outflow observed in H I 21 cm (Morganti et al. 2004a), which in other radio galaxies is observed to be powered by a radio jet. Jets may turn on late in the merger sequence in some ULIRGs as they evolve into unobscured quasars.

The average fraction of neutral outflowing gas that escapes Seyfert 2s and enters the IGM is non-negligible, perhaps as high as 60%. Thus, AGN-dominated ULIRGs are more likely to pollute the intergalactic medium with gas and energy than the starburst-dominated ULIRGs. These outflows will be metal-enriched because of the strong starbursts present in these Seyferts.

(6) Outlook. Since outflows in Seyfert 2 ULIRGs receive substantial momentum and energy injection from a circumnuclear starburst, it would clearly be useful to observe a sample of Seyferts in which the starburst component is minimal in order to better study energy injection from the AGN. Observing Seyferts selected by nuclear X-ray, radio, and/or optical luminosity would allow us to study the absorption-line phase of outflows in a sample of Seyferts that is less biased towards starbursting galaxies. It would be especially useful to compare to a set of galaxies which have well-studied narrow-line regions in emission and/or UV and X-ray absorbers. Ideally, one would also want to select a sample at similar redshifts to those observed here in order to minimize aperture effects.

Another follow-up study suggested by this work is to survey radio-loud Seyferts with Na I D outflows using sensitive, broad-band H I 21 cm observations. This may be one way to directly connect neutral Na to outflowing H I and confirm our outflow mass estimates, as well as to illuminate the physics of energy injection (since radio sources can be studied at high angular resolution). Mrk 231 is a particularly appealing target for this type of study.

A.   APPENDIX: COMMENTS ON INDIVIDUAL OBJECTS

Here we discuss unique properties of individual galaxies based on our spectra.

- **F05024−1941.** The blueshifted Na I D component observed at -1550 km s^{-1} is seen also in Ca II H & K (see Rupke et al. 2002).

- **F08559+1053.** There is an emission-line object $4\rlap{.}''9$ north of the galaxy, possibly related to the faint, compact object seen in the R-band image (Veilleux et al. 2002). No continuum is visible, but several emission lines (elongated and tilted) are, yielding $z = 0.253$. [N II] $\lambda6583$ is not visible but Hα is, suggesting flux(Hα) $\gg$ flux([N II]). [O III] $\lambda5007$ is also brighter than Hβ by an uncertain factor (not more than a few).

- **F13443+0802.** The southwest nucleus of this triplet is listed in Veilleux et al. (1999b) as a Seyfert 2. The Seyfert 2 nucleus is actually the eastern nucleus (and the correct line ratios are listed in Veilleux et al. 1999b under the label of the SW nucleus), while the other two nuclei are an unknown spectral type (SW) and an H II galaxy (NE).

- **F13451+1232**. Veilleux et al. (1999c) claim to observe a broad Paα line in this galaxy. We observe similar asymmetric profiles in the optical in the western nucleus (which hosts most or all of the emission line flux), but they also appear to be present in the [O I] $\lambda\lambda6300$, 6364 forbidden lines (as $2000 - 3000$ km s^{-1} blue wings), which suggests that they do not originate in the broad line region. It is difficult to discern the situation in the east nucleus due to its small separation from the west nucleus, which makes separation of the emission lines from the two nuclei very hard. However, the optical continuum appears to peak in the east nucleus.

REFERENCES

Baum, S. A., O'Dea, C. P., Dallacassa, D., de Bruyn, A. G., & Pedlar, A. 1993, ApJ, 419, 553

Becker, R. H., White, R. L., & Helfand, D. J. 1995, ApJ, 450, 559

Bicknell, G. V., Sutherland, R. S., van Breugel, W. J. M., Dopita, M. A., Dey, A., & Miley, G. K. 2000, ApJ, 540, 678

Boksenberg, A., Carswell, R. F., Allen, D. A., Fosbury, R. A. E., Penston, M. V., & Sargent, W. L. W. 1977, MNRAS, 178, 451

Boroson, T. A., Meyers, K. A., Morris, S. L., & Persson, S. E. 1991, ApJ, 370, L19

Boroson, T. A., & Meyers, K. A. 1992, ApJ, 397, 442

Bryant, P. M., & Scoville, N. Z. 1996, ApJ, 457, 678

Carilli, C. L., & Taylor, G. B. 2000, ApJ, 532, 95

Carilli, C. L., Wrobel, J. M., & Ulvestad, J. S. 1998, AJ, 115, 928

Cecil, G., Bland, J., & Tully, R. B. 1990, ApJ, 355, 70

Colina, L., Arribas, S., & Borne, K. D. 1999, ApJ, 527, 13L

Crenshaw, D. M., & Kraemer, S. B. 2005, ApJ, 625, 680

Crenshaw, D. M., Kraemer, S. B., & George, I. M. 2003, ARA&A, 41, 117

Colbert, E. J. M., Baum, S. A., Gallimore, J. F., O'Dea, C. P., & Christensen, J. A. 1996a, ApJ, 467, 551

Colbert, E. J. M., Baum, S. A., Gallimore, J. F., O'Dea, C. P., Lehnert, M. D., Tsvetanov, Z. I., Mulchaey, J. S., & Caganoff, S. 1996b, ApJS, 105, 75

Colbert, E. J. M., Baum, S. A., O'Dea, C. P., & Veilleux, S. 1998, ApJ, 496, 786

Condon, J. J., Cotton, W. D., Greisen, E. W., Yin, Q. F., Perley, R. A., Taylor, G. B., & Broderick, J. J. 1998, AJ, 115, 1693

de Kool, M., Arav, N., Becker, R. H., Gregg, M. D., White, R. L., Laurent-Muehleisen, S. A., Price, T., & Korista, K. T. 2001, ApJ, 548, 609

De Robertis, M. M., & Osterbrock, D. E. 1984, ApJ, 286, 171

De Robertis, M. M., & Osterbrock, D. E. 1986, ApJ, 301, 727

Downes, D., & Solomon, P. M. 1998, ApJ, 507, 615

Fan, X., et al. 2004, AJ, 128, 515

Farrah, D., Surace, J. A., Veilleux, S., Sanders, D. B., & Vacca, W. D. 2005, ApJ, 626, 70

Forster, K., Rich, R. M., & McCarthy, J. K. 1995, ApJ, 450, 74

Fragile, P. C., Murray, S. D., Anninos, P., & van Breugel, W. 2004, ApJ, 604, 74

Gallagher, S. C., Brandt, W. N., Laor, A., Elvis, M., Mathur, S., Wills, B. J., & Iyomoto, N. 2001, ApJ, 546, 795

Gallagher, S. C., Schmidt, G. D., Smith, P. S., Brandt, W. N., Chartas, G., Hylton, S., Hines, D. C., & Brotherton, M. S. 2005, ApJ, in press (astro-ph/0506616)

García-Lorenzo, B., Arribas, S., & Mediavilla, E. 2001, A&A, 378, 787

Genzel, R., et al. 1998, ApJ, 498, 579

González Delgado, R. M., Leitherer, C., Heckman, T., Lowenthal, J. D., Ferguson, H. C., & Carmelle, R. 1998a, ApJ, 495, 698

González Delgado, R. M., Heckman, T., Leitherer, C., Meurer, G., Krolik, J., Wilson, A. S., Kinney, A., & Koratkar, A. 1998b, ApJ, 505, 174

Hamilton, D., & Keel, W. C. 1987, ApJ, 321, 211

Hamann, F. W., Barlow, T. A., Chaffee, F. C., Foltz, C. B., & Weymann, R. J. 2001, ApJ, 550, 142

Heckman, T. M., Lehnert, M. D., Strickland, D. K., & Armus, L. 2000, ApJS, 129, 493

Hines, D. C., & Wills, B. J. 1995, ApJ, 448, L69

Holt, J., Tadhunter, C. N., & Morganti, R. 2003, MNRAS, 342, 227

Iwasawa, K., Wilson, A. S., Fabian, A. C., & Young, A. J. 2003, MNRAS, 345, 369

Kauffmann, G., et al. 2003, MNRAS, 341, 33

Kennicutt, R. C. 1998, ApJ, 498, 541

Kim, D.-C., & Sanders, D. B. 1998, ApJS, 119, 41

Kim, D.-C., Sanders, D. B., Veilleux, S., Mazzarella, J. M., & Soifer, B. T. 1995, ApJS, 98, 129

Kim, D.-C., Veilleux, S., & Sanders, D. B. 1998, ApJ, 484, 92

Klöckner, H.-R., & Baan, W. A. 2004, A&A, 419, 887

Lanzetta, K. M., Turnshek, D. A, & Sandoval, J. 1993, ApJS, 84, 109

Laureijs, R. J., et al. 2000, A&A, 359, 900

Leitherer, C., et al. 1999, ApJS, 123, 3

Levenson, N. A., Weaver, K. A., & Heckman, T. M. 2001a, ApJS, 133, 269

Levenson, N. A., Weaver, K. A., & Heckman, T. M. 2001b, ApJ, 550, 230

Lindblad, P. O. 1999, A&A Rev., 9, 221

Lípari, S. 1994, ApJ, 436, 102

Lutz, D., Veilleux, S., & Genzel, R. 1999, ApJ, 517, L13

Martin, C. L. 2005, ApJ, 621, 227

McKernan, B., Yaqoob, T., & Reynolds, C. S. 2005, ApJ, in press

Morganti, R., Oosterloo, T. A., Tadhunter, C. N., van Moorsel, G., Killeen, N., & Wills, K. A. 2001, MNRAS, 323, 331

Morganti, R., Oosterloo, T. A., Emonts, B. H. C., Tadhunter, C. N., Holt, J. 2004a, in IAU 217, Recycling Intergalactic and Interstellar Matter, eds. P. A. Duc, J. Braine, & E. Brinks (IAU)

Morganti, R., Oosterloo, T. A., Emonts, B. H. C., van der Hulst, J. M., & Tadhunter, C. N. 2003, ApJ, 593, 69

Morganti, R., Oosterloo, T. A., Tadhunter, C. N., van Moorsel, G., & Emonts, B. 2005, A&A, in press (astro-ph/0505365)

Morganti, R., Oosterloo, T. A., Tadhunter, C. N., Vermeulen, R., Pihlström, Y. M., van Moorsel, G., & Wills, K. A. 2004b, A&A, 424, 119

Morganti, R., Oosterloo, T. A., & Tsvetanov, Z. 1998, AJ, 115, 915

Morganti, R., Tsvetanov, Z. I., Gallimore, J., & Allen, M. G. 1999, A&AS, 137, 457

Mould, J. R., et al. 2000, ApJ, 536, 266

Murray, N., Quartaert, E., & Thompson, T. A. 2005, ApJ, 618, 569

Nagar, N. M., Falcke, H., & Wilson, A. S. 2005, A&A, in press

Nagar, N. M., Wilson, A. S., Falcke, H., Veilleux, S., & Maiolino, R. 2003, A&A, 409, 115

Nelson, C. H., & Whittle, M. 1996, ApJ, 465, 96

Osterloo, T. A., Morganti, R., Tzioumis, A., Reynolds, J., King, E., McCulloch, P., & Tsvetanov, Z. 2000, AJ, 119, 2085

Phillips, A. C. 1993, AJ, 105, 486

Rejkuba, M., Minniti, D., Courbin, F., & Silva, D. R. 2002, ApJ, 564, 688

Reynolds, C. S., Heinz, S., & Begelman, M. C. 2002, MNRAS, 332, 271

Roychowdhury, S., Ruszkowski, M., Nath, B. B., & Begelman, M. C. 2004, ApJ, 615, 681

Rupke, D. S., Veilleux, S., & Sanders, D. B. 2002, ApJ, 570, 588

Rupke, D. S., Veilleux, S., & Sanders, D. B. 2005a, ApJS, in press

Rupke, D. S., Veilleux, S., & Sanders, D. B. 2005b, ApJS, in press

Salzer, J. J., Lee, J. C., Melbourne, J., Hinz, J. L., Alonso-Herrero, A., & Jangren, A. 2005, ApJ, 624, 661

Sanders, D. B., Mazzarella, J. M., Kim, D.-C., Surace, J. A., & Soifer, B. T. 2003, AJ, 126, 1607

Sanders, D. B., Scoville, N. Z., & Soifer, B. T. 1991, ApJ, 370, 158

Sanders, D. B., Soifer, B. T., Elias, J. H., Madore, B. F., Matthews, K., Neugebauer, G., & Scoville, N. Z. 1988, ApJ, 325, 74

Schiano, A. V. R. 1985, ApJ, 299, 24

Schwartz, C. M., & Martin, C. L. 2004, ApJ, 610, 201

Sheinis, A. I., Bolte, M., Epps, H. W., Kibrick, R. I., Miller, J. S., Radovan, M. V., Bigelow, B. C., & Sutin, B. M. 2002, PASP, 114, 851

Springel, V., Di Matteo, T., & Hernquist, L. 2005, ApJ, 520, L79

Stanford, S. A., Stern, D., van Breugel, W., & De Breuck, C. 2000, ApJS, 131, 185

Stanghellini, C., O'Dea, C. P., Baum, S. A., Dallacasa, D., Fanti, R., & Fanti, C. 1997, A&A, 325, 943

Steffen, W., Holloway, A. J., & Pedlar, A. 1996a, MNRAS, 282, 130

Steffen, W., Holloway, A. J., & Pedlar, A. 1996b, MNRAS, 282, 1203

Surace, J. A., Sanders, D. B., Vacca, W. D., Veilleux, S., & Mazzarella, J. M. 1998, ApJ, 492, 116

Tadhunter, C., Robinson, T. G., González Delgado, R. M., Wills, K., & Morganti, R. 2005, MNRAS, 356, 480

Taylor, G. B., Silver, C. S., Ulvestad, J. S., & Carilli, C. L. 1999, ApJ, 519, 185

Ulvestad, J. S., Wrobel, J. M., & Carilli, C. L. 1999, ApJ, 516, 127

Veilleux, S. 1991a, ApJS, 75, 357

Veilleux, S. 1991b, ApJS, 75, 383

Veilleux, S. 1991c, ApJ, 369, 331

Veilleux, S., Bland-Hawthorn, J., Cecil, G., Tully, R. B., & Miller, S. T. 1999a, ApJ, 520, 111

Veilleux, S., Cecil, G., & Bland-Hawthorn, J. 2005, ARA&A, in press (astro-ph/0504435)

Veilleux, S., Kim, D.-C., & Sanders, D. B. 1999b, ApJ, 522, 113

Veilleux, S., Kim, D.-C., & Sanders, D. B. 2002, ApJ, 143, 315

Veilleux, S., Kim, D.-C., Sanders, D. B., Mazzarella, J. M., & Soifer, B. T. 1995, ApJS, 98, 171

Veilleux, S., Sanders, D. B., & Kim, D.-C. 1999c, ApJ, 522, 139

Veilleux, S., Shopbell, P. L., & Miller, S. T. 2001, AJ, 121, 198

Veilleux, S., Shopbell, P. L., Rupke, D. S., Bland-Hawthorn, J., & Cecil, G. 2003, AJ, 26, 2185

Weiner, B. J., et al. 2005, ApJ, 620, 595

Weymann, R. J., Morris, S. L., Foltz, C. B., & Hewett, P. C. 1991, ApJ, 373, 23

Whittle, M. 1992a, ApJS, 79, 49

Whittle, M. 1992b, ApJ, 387, 109

Whittle, M. 1992c, ApJ, 387, 121

Willott, C. J., Rawlings, S., & Grimes, J. A. 2003, ApJ, 598, 909

Worrall, D. M., & Birkinshaw, M. 2004, in Lecture Notes in Physics, Physics of Active Galactic Nuclei at all Scales, eds. D. Alloin, R. Johnson, & P. Lira (Springer Verlag), astro-ph/0410297

Zensus, J. A. 1997, ARA&A, 35, 607
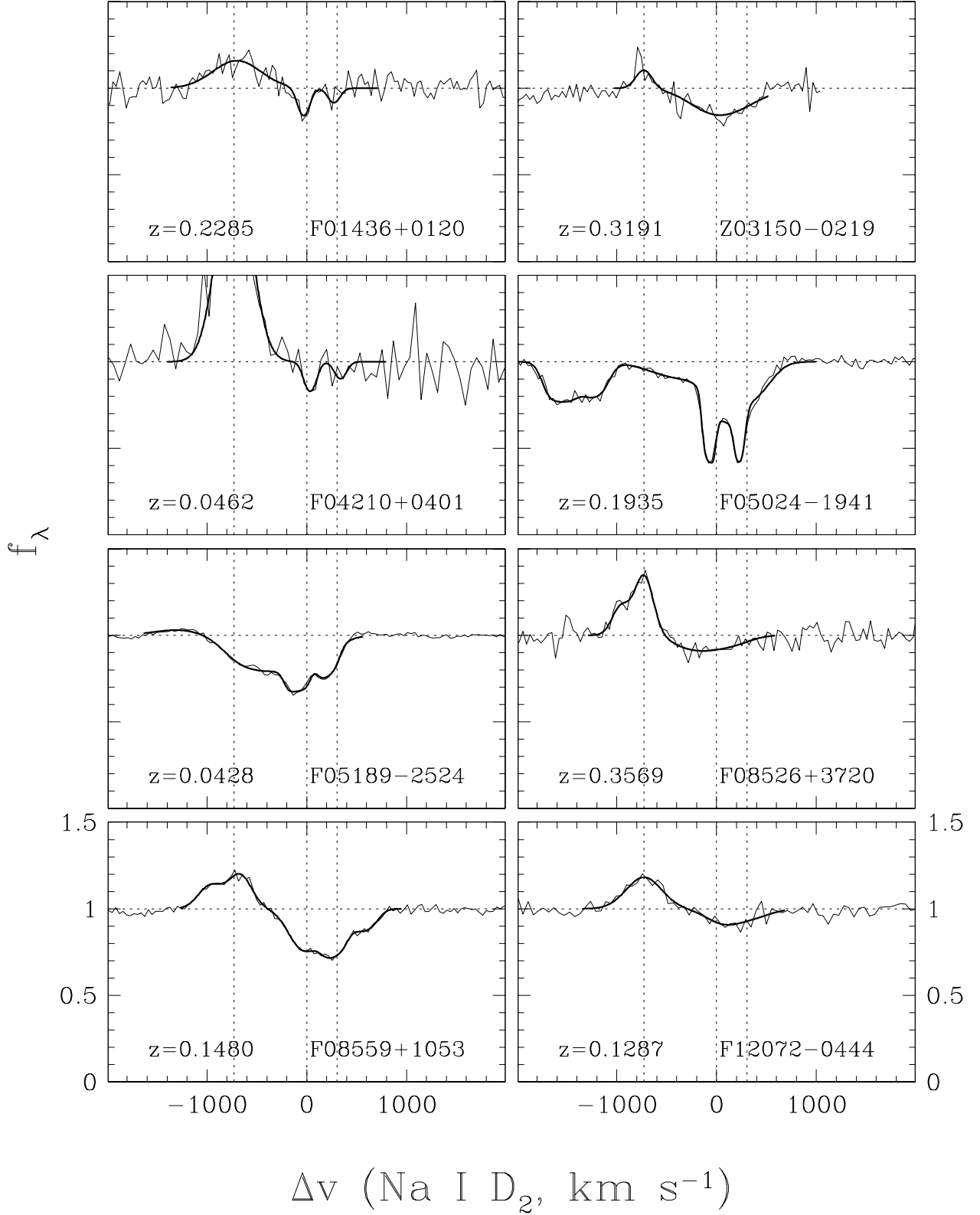
Fig. 1.— Spectra of the Na I D line in infrared-luminous Seyfert 2 galaxies. The thin lines are the (smoothed) original spectra and the thick lines are fits to the data. The vertical dotted lines locate the Na I D $\lambda\lambda5890$, 5896 doublet and He I $\lambda5876$ emission line in the rest frame of the galaxy. The diagonal hashed lines locate atmospheric absorption from O_2.

z=0.3375   F12278+3539

z=0.1486   F13305−1739

z=0.0373   F13428+5608

z=0.1347   F13443+0802:E

z=0.1348   F13443+0802:NE

z=0.1342   F13443+0802:SW

z=0.1218   F13451+1232:W

z=0.1220   F13451+1232:E

f_λ

Δv (Na I D$_2$, km s^{-1})
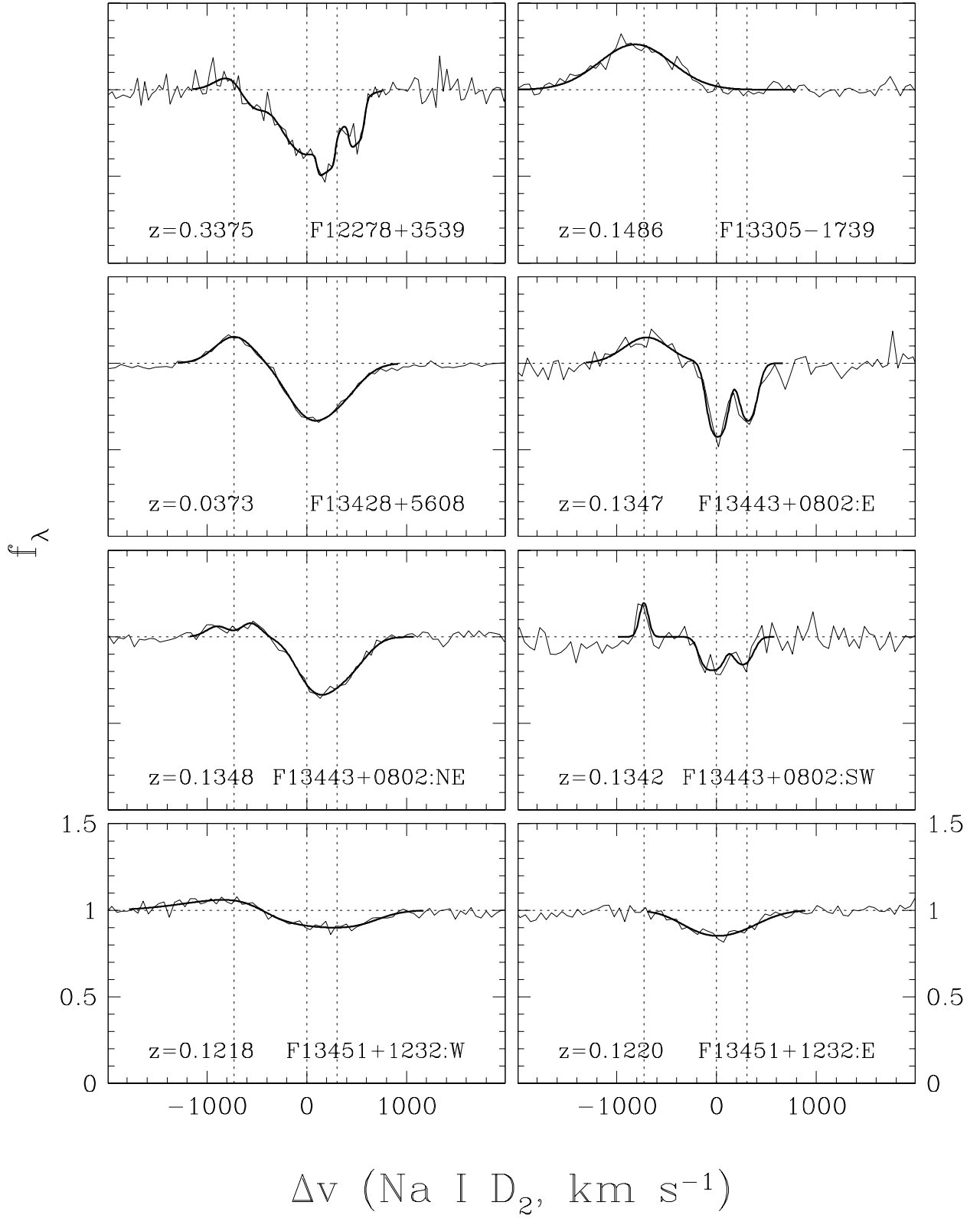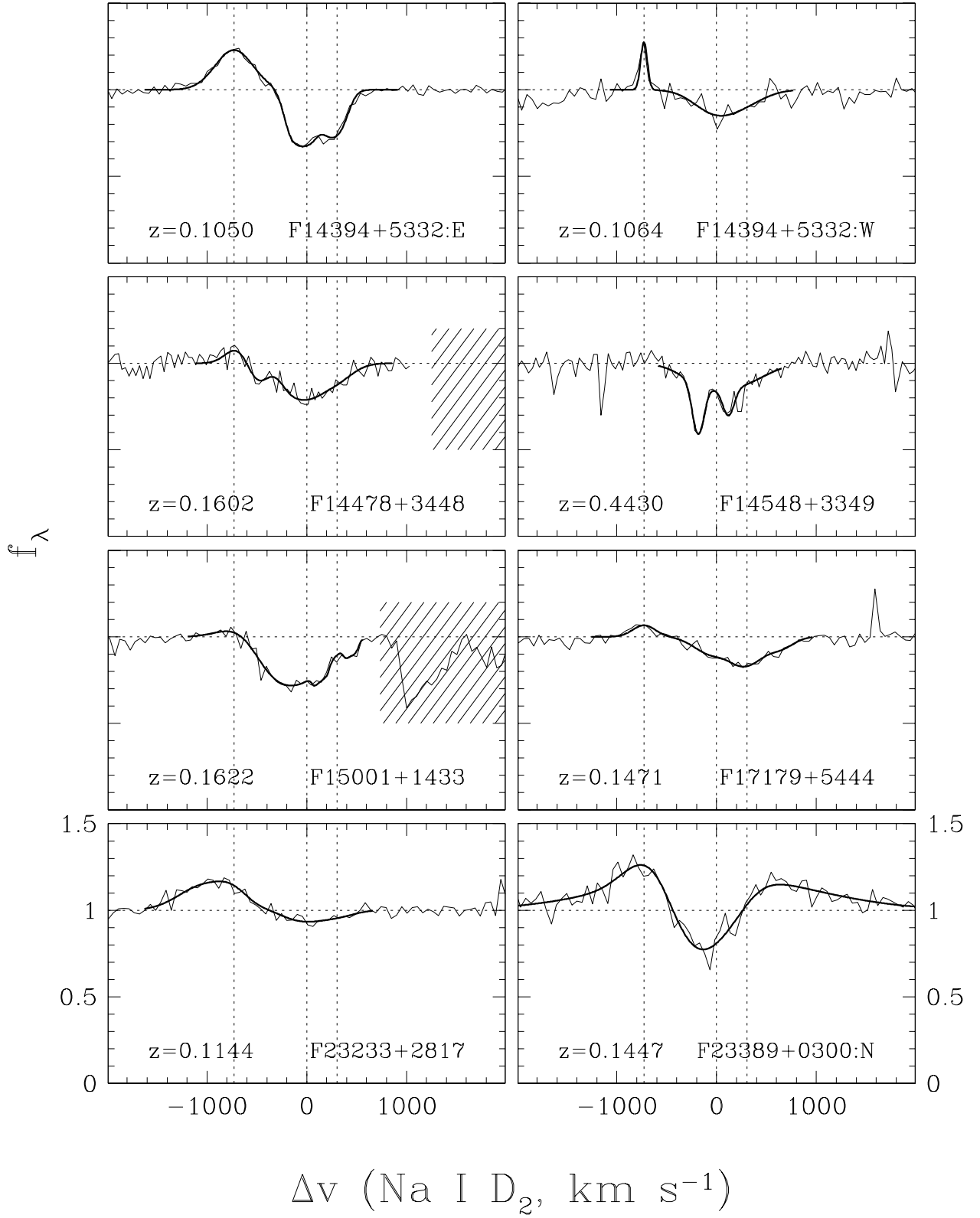
Fig. 1.— *Continued.*
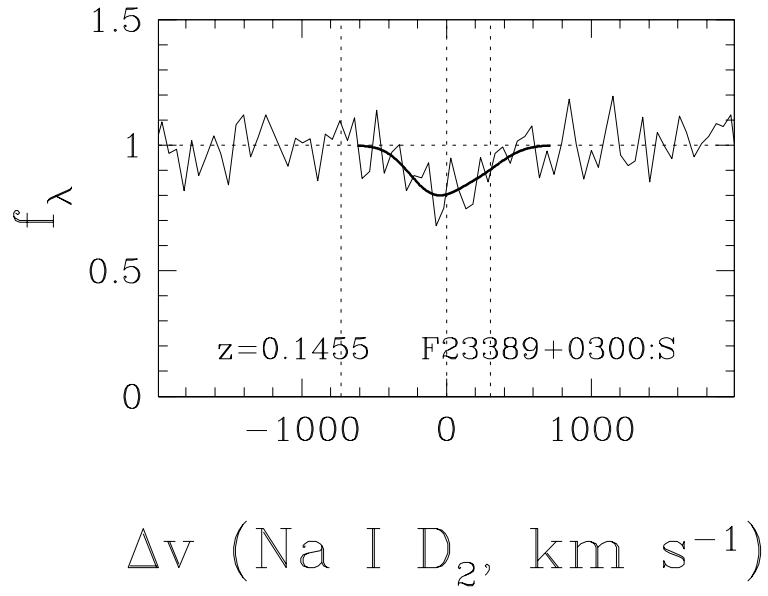
Fig. 1.— *Continued.*

Fig. 1.— *Continued.*
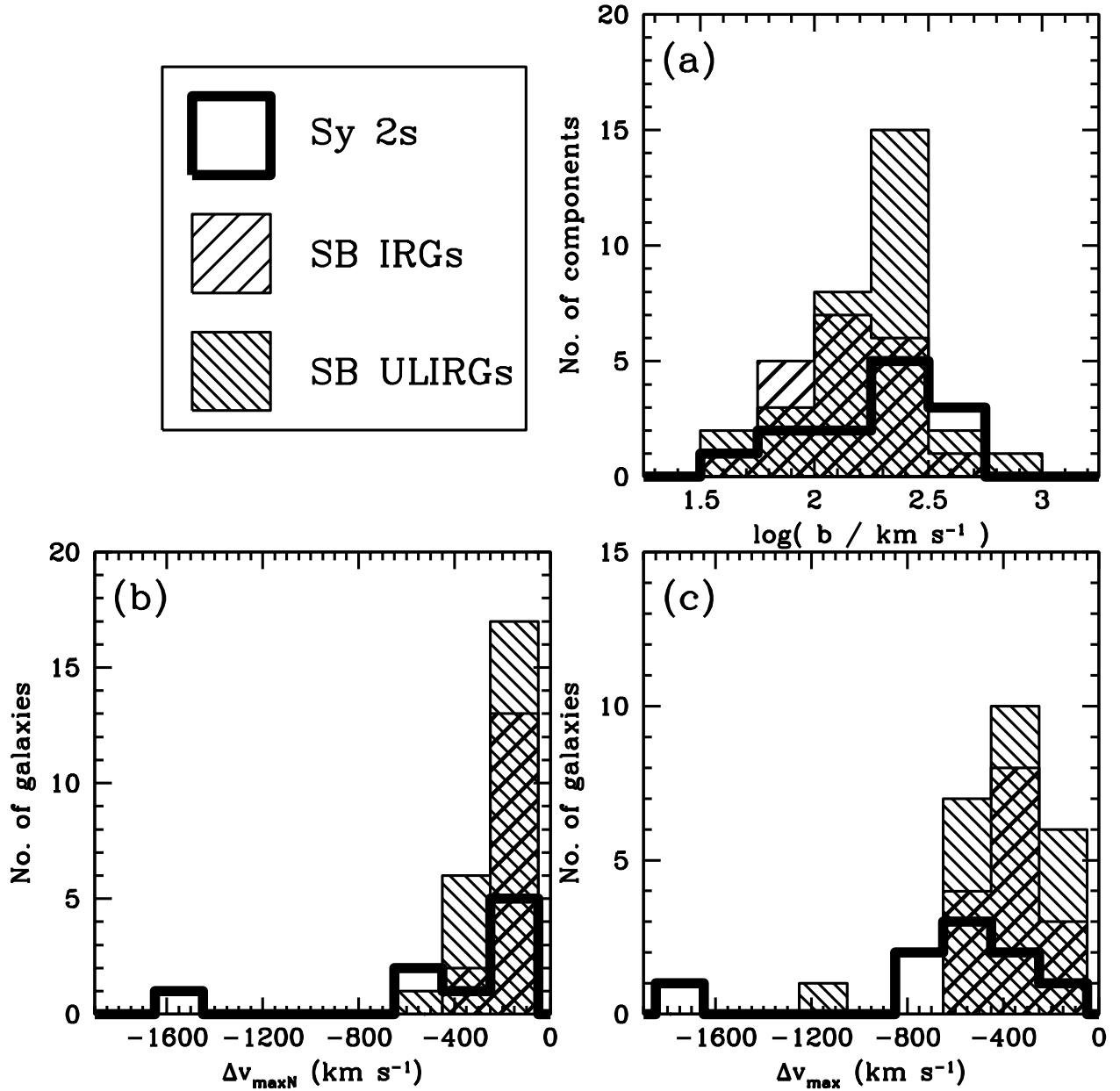
Fig. 2.— Distributions of (a) Doppler parameter, (b) velocity of the highest column density gas, and (c) maximum velocity ($\Delta v_{max} = \Delta v - \text{FWHM}/2$) in Seyfert 2 ULIRGs, infrared-luminous starbursts, and starburst ULIRGs. The starburst data are from Paper II. We used K-S and Kuiper tests to look for significant differences among the different subsamples. Statistically significant differences (P[null] < 0.1 in both tests) exist only in Δv_{maxN}, between the starburst ULIRGs and the starburst IRGs, and between Seyfert 2 ULIRGs and starburst IRGs. See Table 6 for the computed values of P(null), and §3.1 for further discussion.
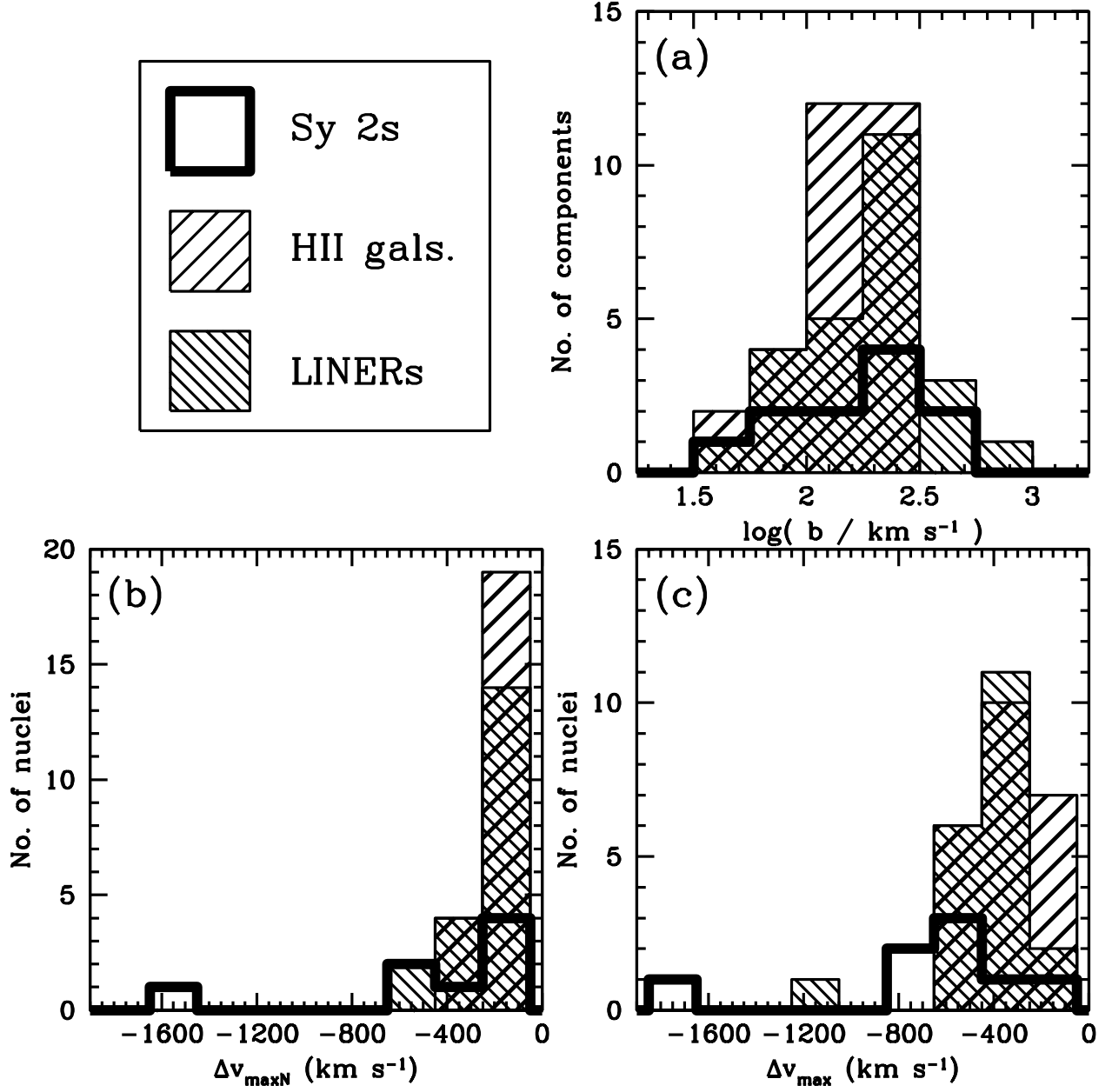
Fig. 3.— Same as Figure 2, but the subsamples compared are the Seyfert 2s, H II galaxies, and LINERs.

−1000   0   1000

Δv (km s^{-1})
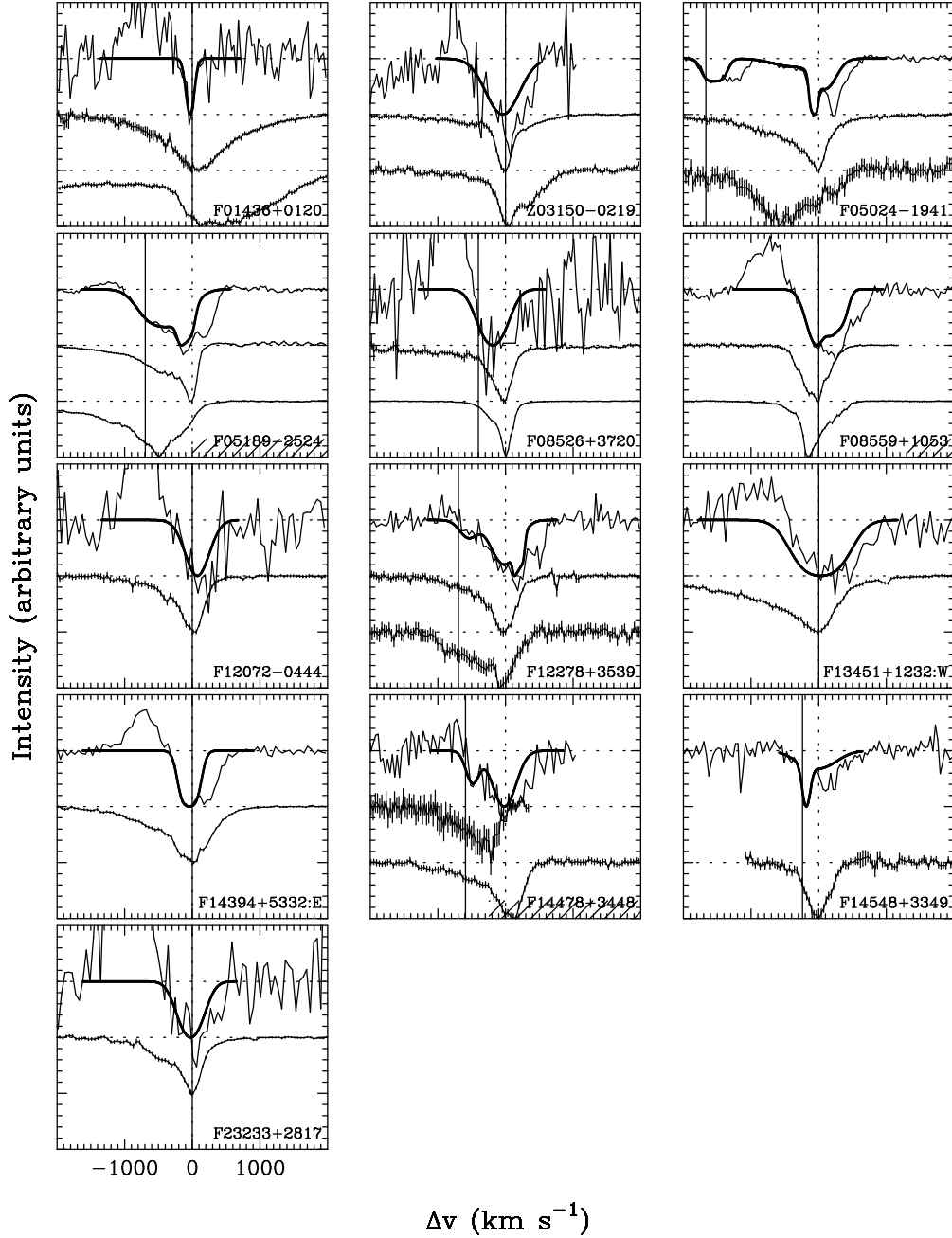
Fig. 4.— Emission-line spectra of 13 infrared-luminous Seyfert 2 galaxies from our sample which have noticeable emission-line asymmetries in the profile wings based on our moderate-resolution data. The top spectrum (red) in each panel is Na I D, with our fit to the Na I D$_2$ $\lambda5890$ line superimposed (green). The velocity scale is relative to systemic in this line. The middle spectrum (blue) is [N II] $\lambda6548$ for $\Delta v < 0$ and (properly scaled) [N II] $\lambda6583$ for $\Delta v > 0$. The bottom spectrum (orange) is [O III] $\lambda5007$. The vertical thick line locates the neutral gas maximum velocity, Δv_{max}. The vertical error bars in the emission-line spectra are 2σ errors. Twelve of these galaxies have a blue emission-line wing (in [O III] and/or [N II]) with a higher maximum velocity and/or more flux than the red wing, plus another three based on low-resolution data, for a total of 15 of 20 Seyfert 2s. See §3.2 for further discussion.
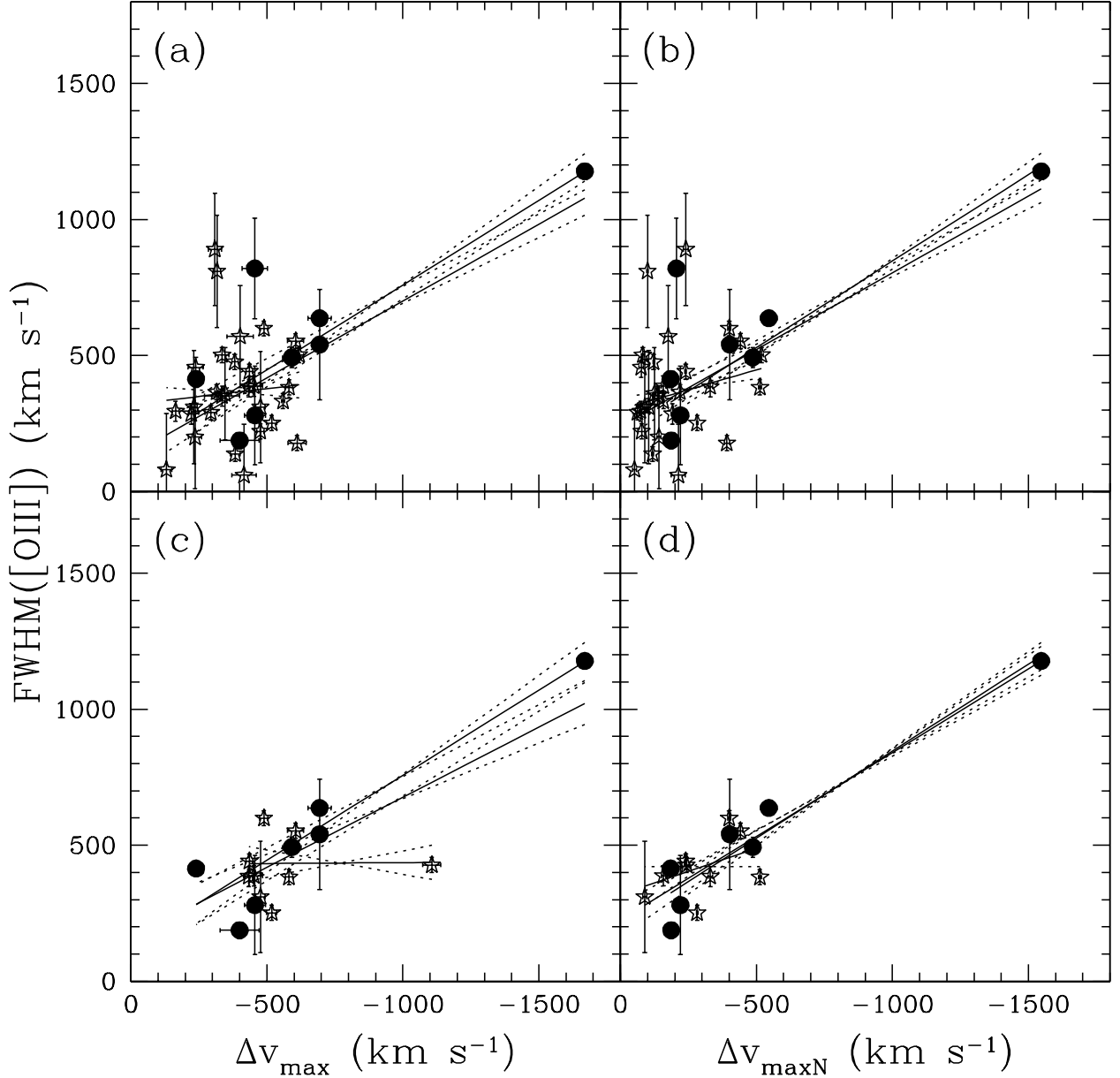
Fig. 5.— Full-width at half-maximum of the [O III] λ5007 emission line as a function of (a) Δv_{max} and (b) Δv_{maxN} for all galaxies with [O III] measurements and (c) Δv_{max} and (d) Δv_{maxN} for just those galaxies with obvious blue emission-line asymmetries (BELA) in [O III] or [N II] $\lambda\lambda$6548, 6583. Open stars (red) represent starbursts from Paper II and filled circles (blue) represent Seyfert 2s. The three solid lines are fits (with 1σ errors shown as dashed lines) to the starbursts and Seyferts separately and to the whole sample. We find no significant correlations in the starburst galaxies alone. When the Seyfert 2s are added, correlations emerge between FWHM([O III]) and Δv_{maxN}, both in all the galaxies and in only those nuclei with BELA. These correlations remain in the absence of the highest-velocity point (F05024−1941). These plots indicate a connection of neutral outflows in Seyfert 2s to the 'extended' narrow-line region (§3.2).
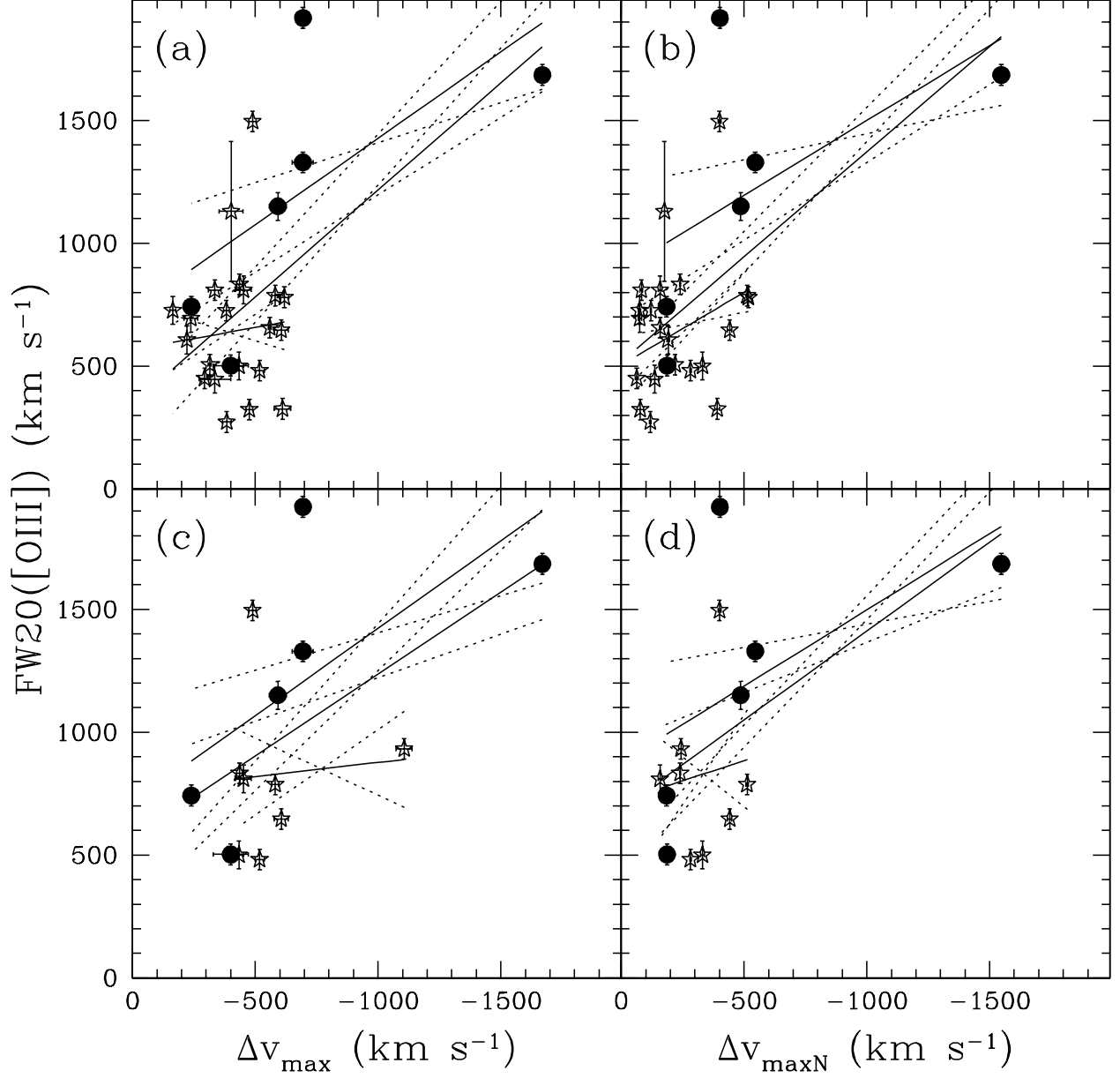
Fig. 6.— Same as Figure 5, but for the full-width at 20% of maximum intensity of the [O III] λ5007 emission line. There are no significant correlations. This implies that the inner narrow-line region in Seyfert 2s, where the high-velocity ionized gas arises, is unconnected with the neutral outflows observed in Na I D (§3.2).
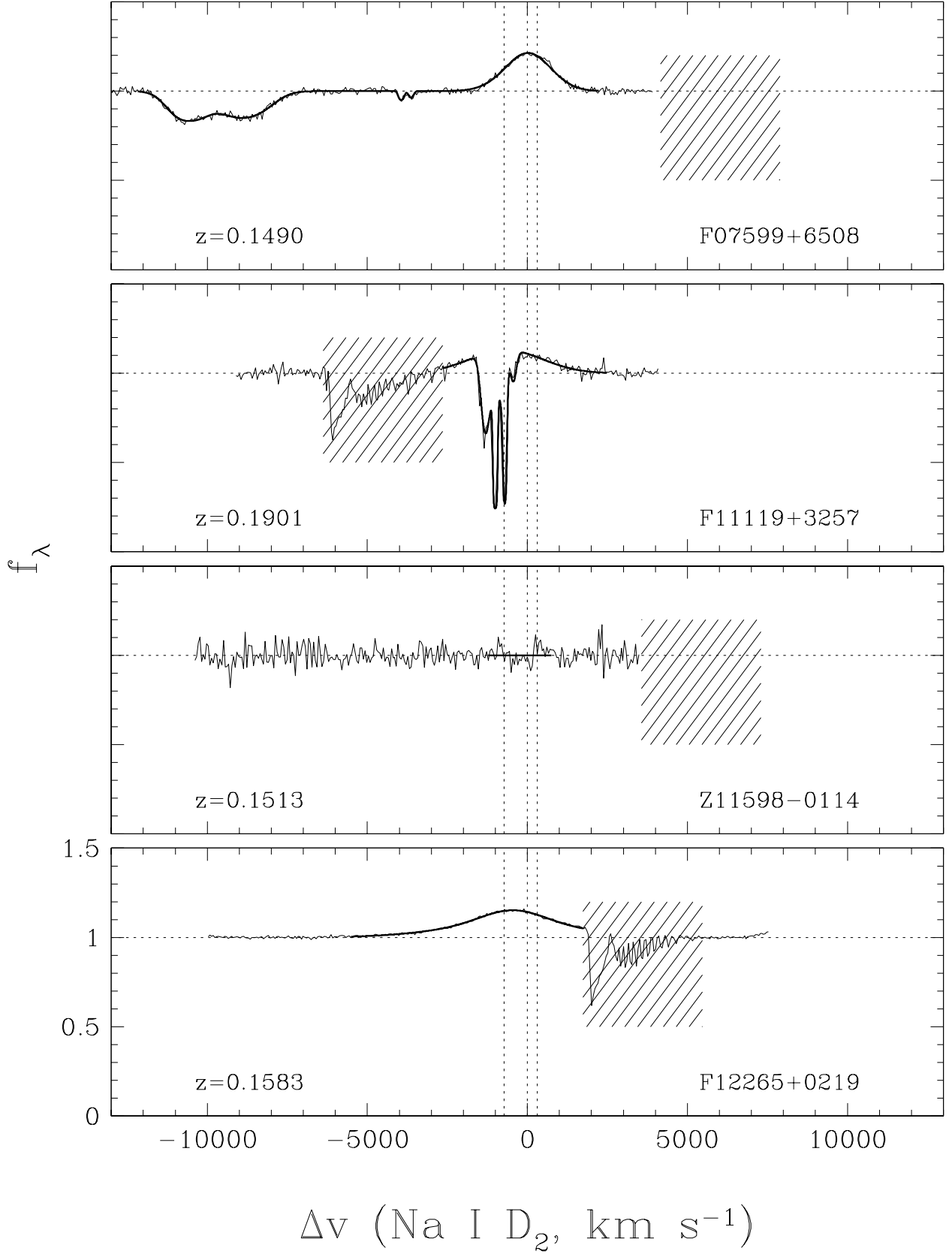
Fig. 7.— Spectra of the Na I D line in Seyfert 1 ULIRGs. See Figure 1 for more details.
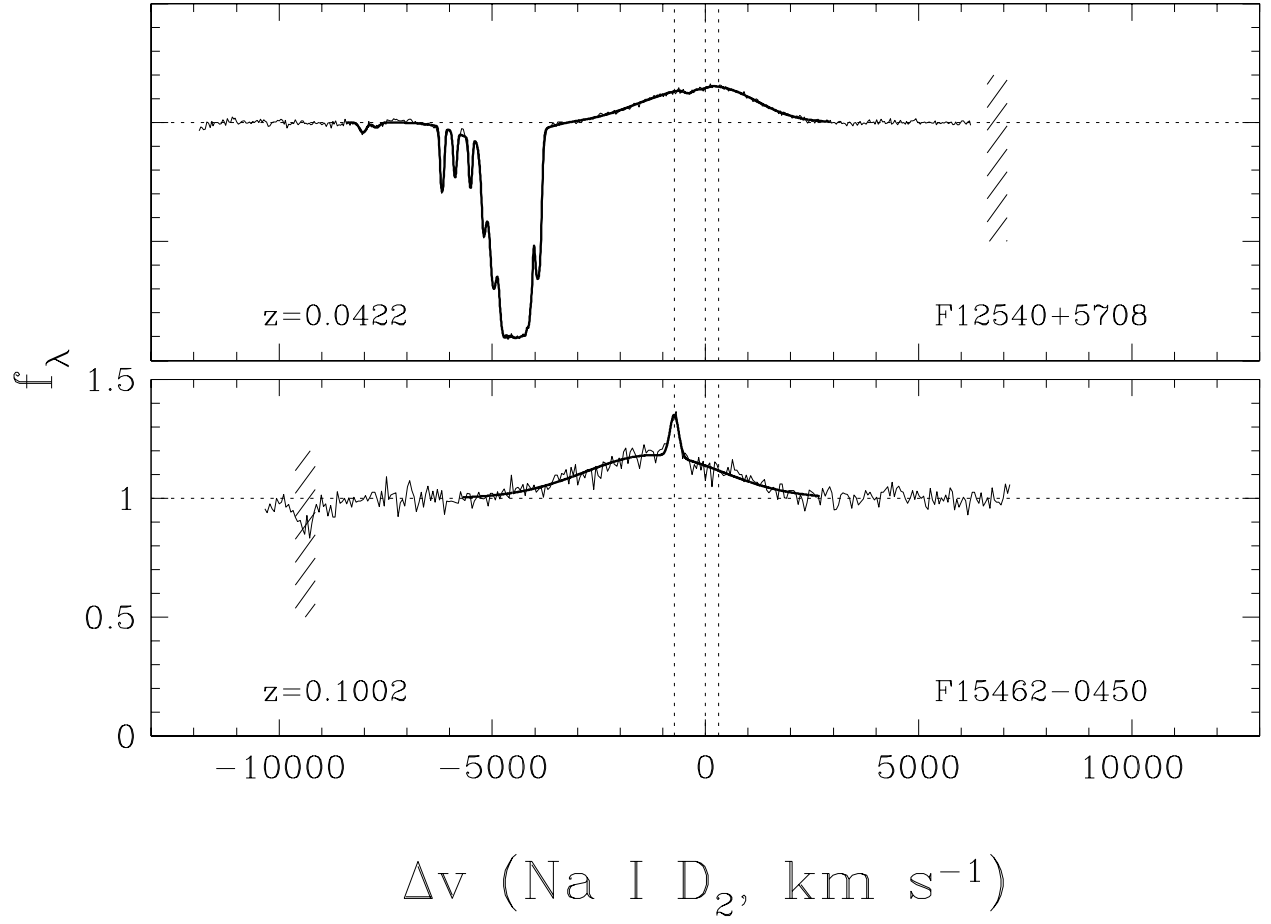
Fig. 7.— *Continued.*
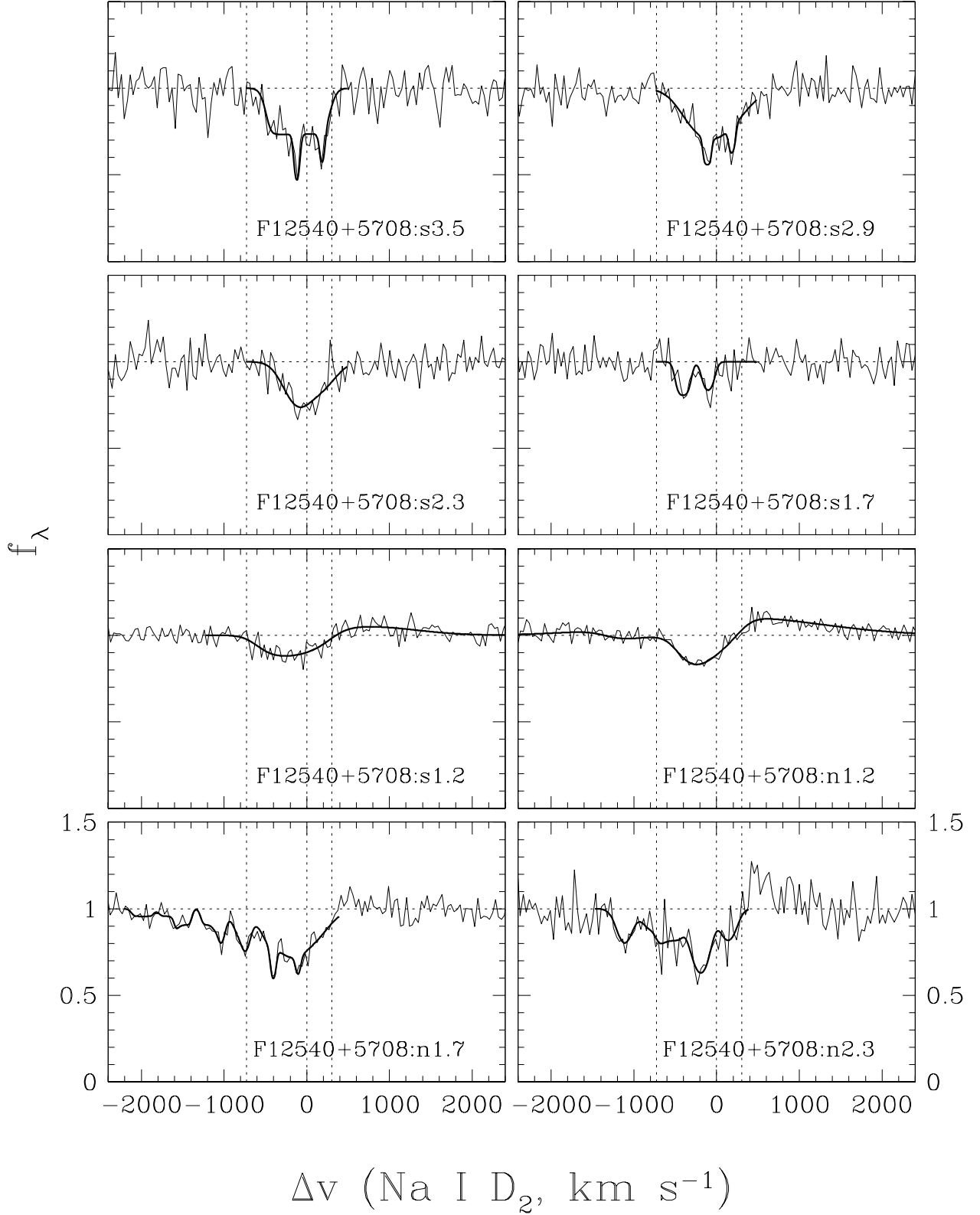
Fig. 8.— Spectra of low-velocity, extended Na I D emission in Mrk 231 along the north-south slit. The aperture labels indicate position, in kpc, relative to the nucleus (s = south, n = north). See Figure 1 for more details. Further discussion of Mrk 231 is in §5.
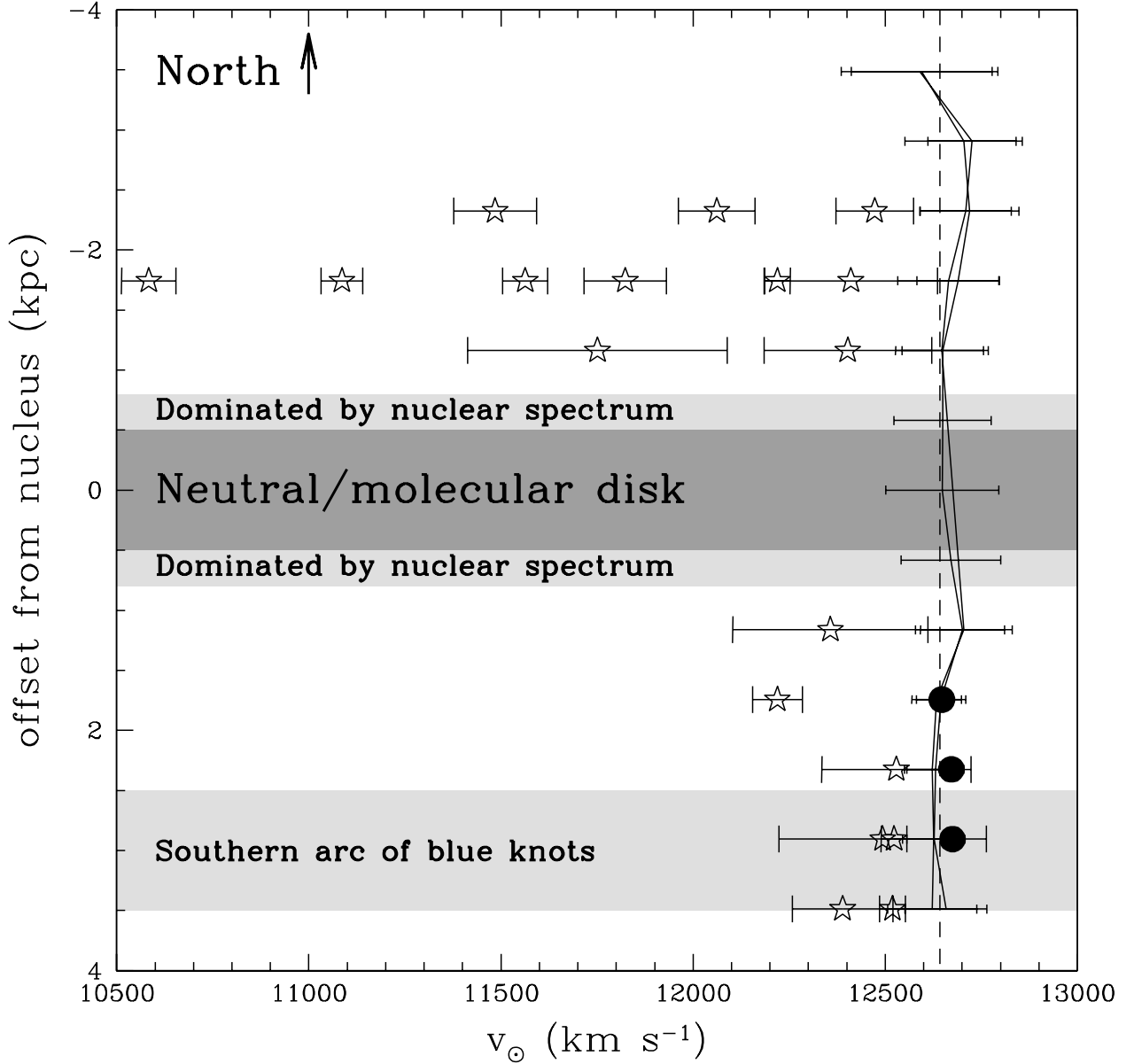
Fig. 9.— Velocities of emission and absorption lines in Mrk 231 along the north-south slit (north is up). The vertical dashed line is the systemic velocity of the nucleus from H I and CO data (Carilli et al. 1998; Sanders et al. 1991). The jagged vertical lines show the velocities of the narrow component of Hα (red) and [S II] λλ6716, 6731 (black). The closed circles (green) show the velocity of the Ca II triplet. Open stars (blue) locate outflowing Na I D components. Error bars on the emission and absorption components show their FWHM. The shaded regions locate the regions dominated by the nuclear spectrum in the three central bins, as well as the location and extent of the nuclear H I/CO disk and the southern arc of blue star-forming knots. The best model for these data as well as the emission lines in Mrk 231 is a wide-angle wind; see §5 for further discussion.
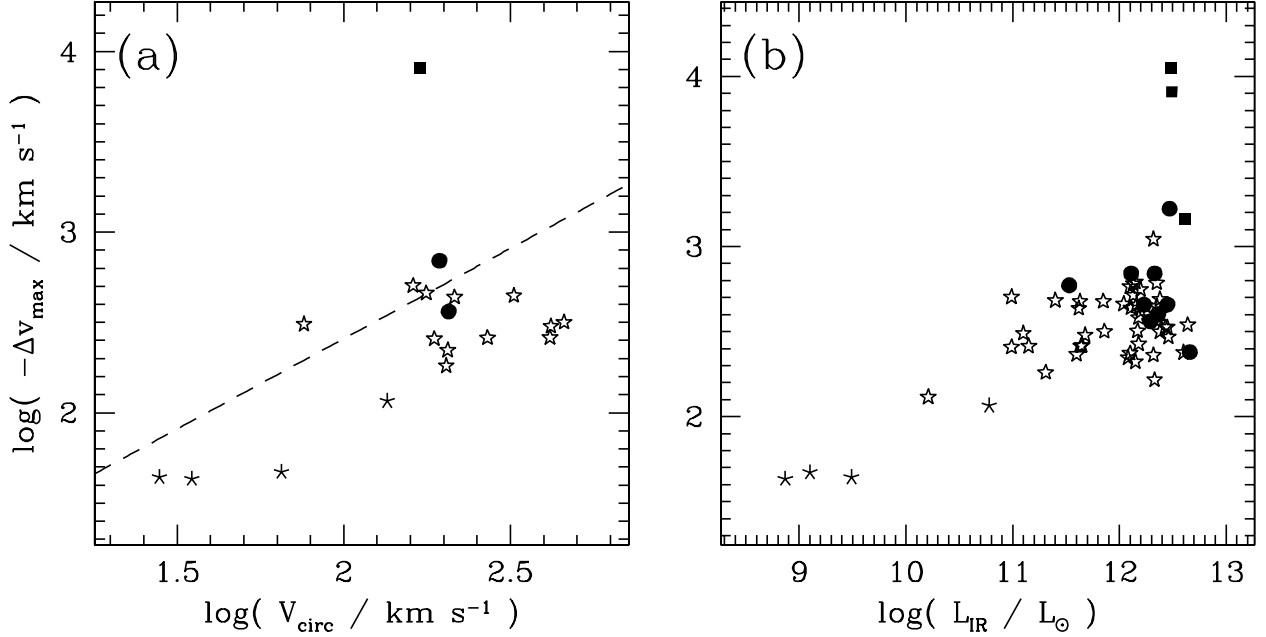
Fig. 10.— Maximum outflow velocity vs. (a) circular velocity and (b) infrared luminosity. Skeletal stars (red) are dwarf galaxies from Schwartz & Martin (2004); open stars (red) are infrared-luminous starbursts from Paper II; closed circles (blue) are Seyfert 2s; and closed squares (black) are Seyfert 1s. Note that the phase-space locations of starburst ULIRGs and Seyfert 2 ULIRGs are not significantly different. The dashed line in (a) is the escape velocity of a singular isothermal sphere at a radius $r = 0.1 r_{max}$. See §6.2 for more discussion.
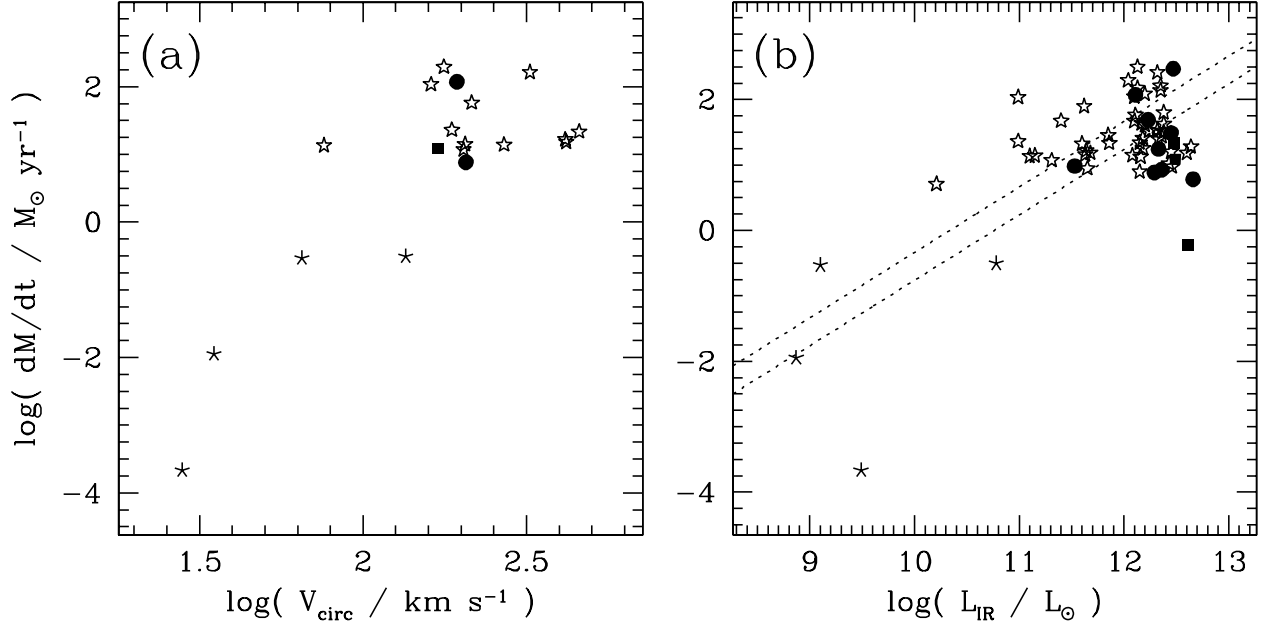
Fig. 11.— Mass outflow rate vs. (a) circular velocity and (b) infrared luminosity. Symbols are as in Figure 10. The mass outflow rates are computed assuming an outflow radius of 5 kpc for the Seyfert 2 ULIRGs and starbursts, 10 pc for the Seyfert 1s, and a varying radius for the dwarfs (Schwartz & Martin 2004). Note that the phase-space locations of starburst ULIRGs and Seyfert 2 ULIRGs are not significantly different. The short-dashed lines in (b) represent the injected hot gas mass outflow rate from stellar winds and supernovae for a continuous starburst of age $\gtrsim$40 Myr, assuming twice solar metallicity and a Salpeter IMF $(1 - 100\ M_\odot$; Leitherer et al. 1999). We assume a conversion from L_{IR} to SFR such that the starburst powers 80% (for the starburst ULIRGs; top line) and 30% (for the Seyfert ULIRGs; bottom line) of L_{IR} (§2.3). See §6.2 for more discussion.
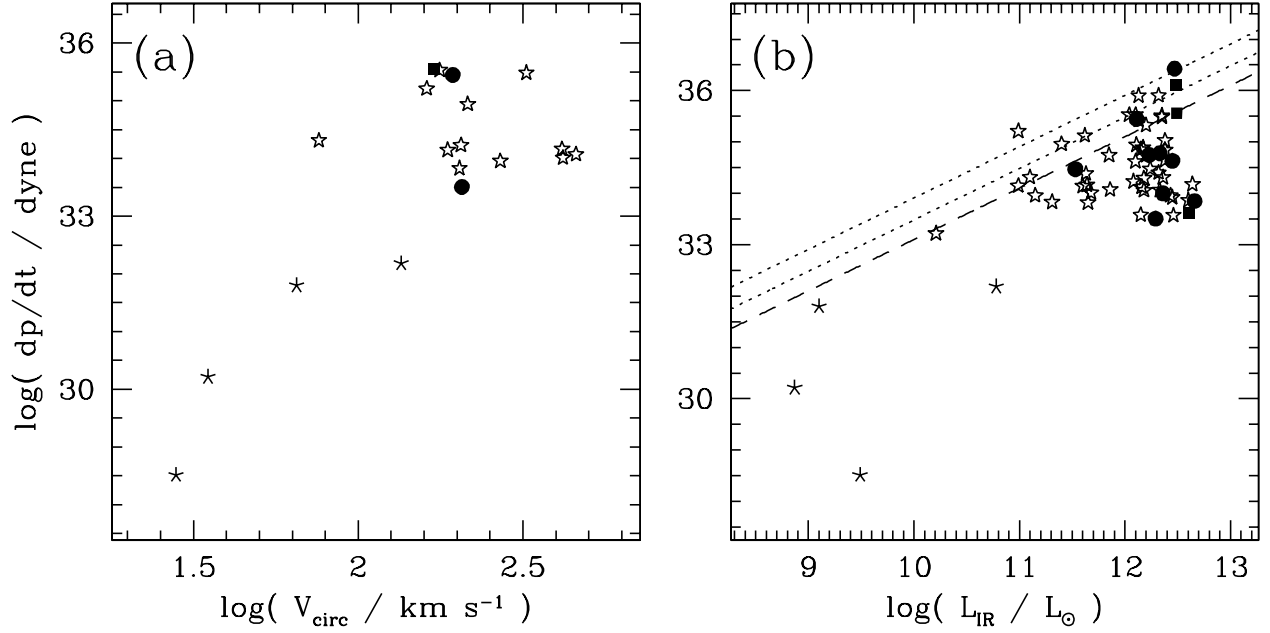
Fig. 12.— Same as Figure 11, but for momentum outflow rate. The long-dashed line in (b) is the momentum injection rate from radiation pressure, assuming isotropic absorption of the bolometric luminosity of the galaxy by optically thick clouds. Note that the phase-space locations of starburst ULIRGs and Seyfert 2 ULIRGs are not significantly different. Note also that the momentum from the starburst is in each case (except perhaps one) sufficient to power the outflow, implying that the momentum injection into the outflow from the AGN is similar to or less than that from the starburst. See §6.2 for more discussion.
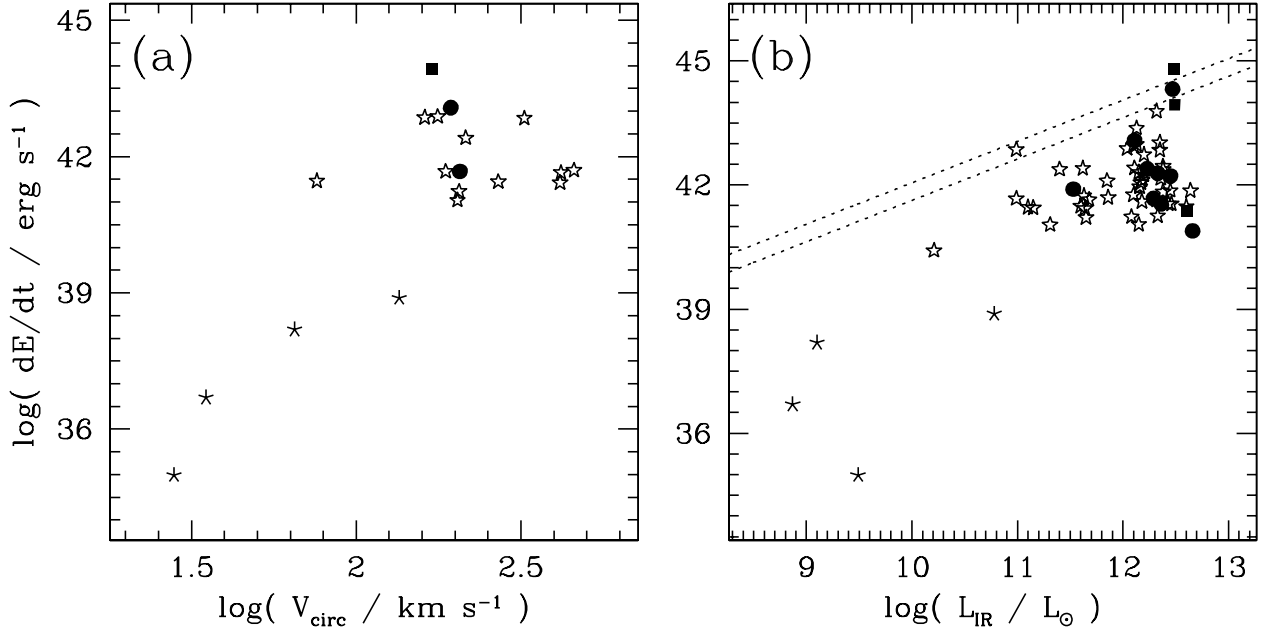
Fig. 13.— Same as Figure 11, but for energy outflow rate. Note that the phase-space locations of starburst ULIRGs and Seyfert 2 ULIRGs are not significantly different, and that the energy from the starburst is sufficient to drive the outflow (implying that the energy in the outflow originating from the AGN is comparable to that originating from the starburst). Furthermore, on average, Seyfert 2s and starbursts have approximately the same mechanical luminosity per unit radiative luminosity. See §6.2 for more discussion.

Table 1.   Galaxy Properties

Name (1)	Other (2)	z (3)	Type (4)	L_{IR} (5)	SFR (6)	v_c (7)	W_{eq} (8)	Run (9)	t_{exp} (10)	PA (11)	Refs (12)
Seyfert 2s											
F01436+0120	$\cdots$	0.2285	S2	11.83	47	$\cdots$	0.58	MMT/2002dec31	3600	0	2
Z03150−0219	$\cdots$	0.3191	S2	12.30	138	$\cdots$	2.21	Keck/2002jan17,MMT/2002dec31	9000	0	2
F04210+0401	$\cdots$	0.0462	S2	11.14	7	$\cdots$	0.64	KPNO/2003sep26	1800	0	4
F05024−1941	$\cdots$	0.1935	S2	12.47	206	$\cdots$	8.87	Keck/2001feb27	1800	0	1
F05189−2524	$\cdots$	0.0428	S2	12.11	67	194	5.40	Keck/2001feb28	900	0	13
F08526+3720	$\cdots$	0.3569	S2	12.36	118	$\cdots$	1.24	Keck/2002jan17	1800	0	2
F08559+1053	$\cdots$	0.1480	S2	12.24	120	$\cdots$	3.80	Keck/2001jan24	1200	0	1
F12072−0444	$\cdots$	0.1287	S2	12.37	163	$\cdots$	1.04	KPNO/2004apr14	10800	8	1
F12278+3539	$\cdots$	0.3375	S2	12.33	147	$\cdots$	6.70	Keck/2002mar15	3600	0	2
F13305−1739	$\cdots$	0.1486	S2	12.25	122	$\cdots$	0.00	KPNO/2004apr17	3600	0	1
F13428+5608	Mrk.273	0.0373	S2	12.09	84	399	4.43	KPNO/2004apr15	6000	30	1
F13443+0802:E	$\cdots$	0.1347	S2	12.20	109	$\cdots$	3.02	KPNO/2004apr13,KPNO/2004apr17	14400	166,62	1
F13443+0802:NE	$\cdots$	0.1348	H	$\cdots$	$\cdots$	$\cdots$	4.18	$\cdots$	$\cdots$	$\cdots$	1
F13443+0802:SW	$\cdots$	0.1342	L	$\cdots$	$\cdots$	$\cdots$	1.61	$\cdots$	$\cdots$	$\cdots$	1
F13451+1232:W	4C.12.50	0.1218	S2	12.29	101	236	2.45	KPNO/2004apr14	10800	104	1
F13451+1232:E	$\cdots$	0.1220	$\cdots$	$\cdots$	$\cdots$	206	2.35	$\cdots$	$\cdots$	$\cdots$	1
F14394+5332:E	$\cdots$	0.1050	S2	12.05	77	$\cdots$	3.57	KPNO/2004apr15	9000	93	1
F14394+5332:W	$\cdots$	0.1064	$\cdots$	$\cdots$	$\cdots$	$\cdots$	1.90	$\cdots$	$\cdots$	$\cdots$	1
F14478+3448	$\cdots$	0.1602	S2	11.53	23	$\cdots$	2.96	MMT/2003jun04	7200	270	2
F14548+3349	$\cdots$	0.4430	S2	12.66	315	$\cdots$	3.52	Keck/2002feb16	3600	0	2
F15001+1433	$\cdots$	0.1622	S2	12.45	195	$\cdots$	4.19	KPNO/2004apr13,KPNO/2004apr16	10800	55	1
F17179+5444	$\cdots$	0.1471	S2	12.26	124	$\cdots$	2.40	KPNO/2003sep29	7200	100	1
F23233+2817	$\cdots$	0.1144	S2	12.07	82	$\cdots$	0.82	KPNO/2003sep29	7200	75	1
F23389+0300:N	4C.03.60	0.1447	S2	12.23	117	$\cdots$	4.99	KPNO/2003sep29	7200	12	1
F23389+0300:S	$\cdots$	0.1455	$\cdots$	$\cdots$	$\cdots$	$\cdots$	2.23	$\cdots$	$\cdots$	$\cdots$	1
Seyfert 1s											

Table 1—Continued

Name (1)	Other (2)	z (3)	Type (4)	$L_{\rm IR}$ (5)	SFR (6)	v_c (7)	W_{eq} (8)	Run (9)	t_{exp} (10)	PA (11)	Refs (12)
F07599+6508	$\cdots$	0.1490	S1	12.48	157	$\cdots$	2.43	KPNO/2004apr13	5400	168	1
F11119+3257	$\cdots$	0.1901	S1	12.61	211	$\cdots$	6.85	KPNO/2004apr13	9000	95	1a
Z11598−0114	$\cdots$	0.1513	S1	12.51	166	$\cdots$	0.00	KPNO/2004apr16	3600	12	1
F12265+0219	3C.273	0.1583	S1	12.75	294	$\cdots$	0.00	KPNO/2004apr16	2400	40	1
F12540+5708	Mrk.231	0.0422	S1	12.49	161	170	21.44	Keck/2001feb28,KPNO/2004apr16	5100	0	13
F15462−0450	$\cdots$	0.1002	S1	12.17	77	$\cdots$	0.00	KPNO/2004apr14,KPNO/2004apr15	8400	30	1

References. — (1) Kim & Sanders 1998; Veilleux et al. 1999b; (2) Stanford et al. 2000; (3) Sanders et al. 2003; (4) Kim et al. 1995; Veilleux et al. 1995; (a) Heckman et al. 2000.

Note. — Col.(1): *IRAS* Faint Source Catalog label, plus nuclear ID (e.g., N = north). Col.(2): Another name. Col.(3): Heliocentric redshift. Col.(4): Optical spectral type (§2.4). Col.(5): Infrared luminosity, in logarithmic units of $L_\odot$. Col.(6): Star formation rate, computed from the infrared luminosity using a correction for AGN contribution to $L_{\rm IR}$ (§2.3). Col.(7): Measured circular velocity, equal to $\sqrt{2\sigma^2 + v_{rot}^2}$ (K. Dasyra, private communication). Col.(8): Rest-frame equivalent width of Na I D in Å, as computed from our model fits. Col.(9): Observing run (§2.2). Instruments used were: ESI on Keck, the Red Channel Spectrograph on the MMT, and the R-C Spectrograph on the KPNO 4m. Col.(10): Total exposure time in seconds. Col.(11): Slit position angle. Col.(12): Reference. Numbered references are infrared survey references; lettered references are previous superwind surveys.

Table 2.   Outflow Component Properties

Name (1)	$\lambda_{1,c}$ (2)	Δv (3)		b (4)		$\tau_{1,c}$ (5)		C_f (6)		N(Na I) (7)	N(H) (8)
Seyfert 2s											
F01436+0120	7244.37	-32	($\pm$ 5)	67	($\pm$ 16)	0.09	$\left(^{+0.04}_{-0.01}\right)$	1.00	$\left(^{+0.00}_{-0.00}\right)$	12.32	19.61
Z03150−0219	7778.40	-41	($\pm$ 8)	338	($\pm$ 37)	0.07	$\left(^{+0.03}_{-0.00}\right)$	1.00	$\left(^{+0.00}_{-0.00}\right)$	12.90	20.20
F04210+0401	6170.61	18	($\pm$ 17)	63	($\pm$ 45)	0.32	$\left(^{+\infty}_{-0.14}\right)$	0.36	$\left(^{+0.44}_{-0.02}\right)$	>12.85	>20.19
F05024−1941	7002.50	-1547	($\pm$ 2)	146	($\pm$ 7)	2.00	$\left(^{+0.18}_{-0.16}\right)$	0.24	$\left(^{+0.02}_{-0.02}\right)$	14.02	21.31
$\cdots$	7030.36	-357	($\pm$ 34)	398	($\pm$ 72)	0.27	$\left(^{+0.20}_{-0.04}\right)$	0.19	$\left(^{+0.15}_{-0.03}\right)$	13.58	20.88
$\cdots$	7036.97	-75	($\pm$ 1)	38	($\pm$ 4)	1.93	$\left(^{+0.23}_{-0.12}\right)$	0.46	$\left(^{+0.05}_{-0.03}\right)$	13.42	20.72
$\cdots$	7041.06	99	($\pm$ 6)	209	($\pm$ 16)	0.17	$\left(^{+0.02}_{-0.01}\right)$	1.00	$\left(^{+0.00}_{-0.00}\right)$	13.11	20.40
F05189−2524	6141.44	-402	($\pm$ 3)	351	($\pm$ 7)	1.21	$\left(^{+0.06}_{-0.05}\right)$	0.22	$\left(^{+0.01}_{-0.01}\right)$	14.18	21.54
$\cdots$	6147.79	-92	($\pm$ 1)	91	($\pm$ 3)	2.48	$\left(^{+0.23}_{-0.20}\right)$	0.16	$\left(^{+0.01}_{-0.01}\right)$	13.90	21.26
F08526+3720	7997.42	-187	($\pm$ 20)	256	($\pm$ 82)	0.56	$\left(^{+\infty}_{-0.16}\right)$	0.12	$\left(^{+0.21}_{-0.04}\right)$	>13.71	>21.01
F08559+1053	6769.69	-31	($\pm$ 7)	197	($\pm$ 14)	0.15	$\left(^{+0.04}_{-0.01}\right)$	0.92	$\left(^{+0.06}_{-0.01}\right)$	13.01	20.31
$\cdots$	6776.83	285	($\pm$ 5)	126	($\pm$ 15)	1.13	$\left(^{+0.24}_{-0.11}\right)$	0.17	$\left(^{+0.04}_{-0.02}\right)$	13.70	21.00
F12072−0444	6658.21	74	($\pm$ 26)	239	($\pm$ 68)	0.04	$\left(^{+0.12}_{-0.01}\right)$	0.96	$\left(^{+0.02}_{-0.00}\right)$	12.58	19.89
F12278+3539	7873.64	-546	($\pm$ 31)	178	($\pm$ 35)	0.07	$\left(^{+0.15}_{-0.01}\right)$	1.00	$\left(^{+0.00}_{-0.00}\right)$	12.65	19.95
$\cdots$	7887.57	-16	($\pm$ 10)	246	($\pm$ 30)	0.31	$\left(^{+0.06}_{-0.03}\right)$	0.72	$\left(^{+0.14}_{-0.07}\right)$	13.44	20.74
$\cdots$	7893.11	195	($\pm$ 2)	42	($\pm$ 5)	5.00	$\left(^{+\infty}_{-0.28}\right)$	0.23	$\left(^{+0.01}_{-0.01}\right)$	>13.88	>21.17
F13305−1739	$\cdots$	$\cdots$	$\cdots$	$\cdots$	$\cdots$	$\cdots$	$\cdots$	$\cdots$	$\cdots$	$\cdots$	$\cdots$
F13428+5608	6118.06	29	($\pm$ 3)	285	($\pm$ 15)	0.23	$\left(^{+0.03}_{-0.01}\right)$	0.78	$\left(^{+0.09}_{-0.04}\right)$	13.37	20.73
F13443+0802:E	6692.21	11	($\pm$ 3)	89	($\pm$ 9)	1.28	$\left(^{+0.25}_{-0.18}\right)$	0.46	$\left(^{+0.09}_{-0.06}\right)$	13.61	20.91
F13443+0802:NE	6695.18	105	($\pm$ 4)	248	($\pm$ 19)	0.30	$\left(^{+0.05}_{-0.03}\right)$	0.68	$\left(^{+0.11}_{-0.06}\right)$	13.42	20.72
F13443+0802:SW	6687.87	-43	($\pm$ 14)	99	($\pm$ 33)	1.56	$\left(^{+\infty}_{-0.60}\right)$	0.20	$\left(^{+0.61}_{-0.08}\right)$	>13.74	>21.04

Table 2—Continued

Name (1)	$\lambda_{1,c}$ (2)	Δv (3)		b (4)		$\tau_{1,c}$ (5)		C_f (6)		$N(\mathrm{Na\,I})$ (7)	$N(\mathrm{H})$ (8)
F13451+1232:W	6616.51	28	(± 23)	400	(±101)	1.18	$\left(^{+1.05}_{-0.45}\right)$	0.11	$\left(^{+0.10}_{-0.04}\right)$	14.22	21.52
F13451+1232:E	6615.59	-67	(± 13)	357	(± 71)	0.27	$\left(^{+0.21}_{-0.05}\right)$	0.29	$\left(^{+0.22}_{-0.05}\right)$	13.54	20.83
F14394+5332:E	6515.87	-43	(± 3)	134	(± 9)	1.66	$\left(^{+0.21}_{-0.17}\right)$	0.34	$\left(^{+0.04}_{-0.03}\right)$	13.90	21.20
F14394+5332:W	6524.51	-17	(± 18)	286	(± 72)	0.07	$\left(^{+0.08}_{-0.01}\right)$	1.00	$\left(^{+0.00}_{-0.00}\right)$	12.83	20.13
F14478+3448	6831.25	-487	(± 14)	127	(± 37)	0.06	$\left(^{+\infty}_{-0.01}\right)$	0.99	$\left(^{+0.01}_{-0.00}\right)$	>12.41	>19.75
⋯	6841.92	-19	(± 13)	228	(± 37)	0.12	$\left(^{+0.05}_{-0.02}\right)$	0.85	$\left(^{+0.09}_{-0.03}\right)$	13.00	20.34
F14548+3349	8504.94	-185	(± 2)	66	(± 9)	0.20	$\left(^{+0.05}_{-0.01}\right)$	1.00	$\left(^{+0.00}_{-0.00}\right)$	12.66	19.96
⋯	8509.28	-32	(± 14)	347	(± 68)	0.37	$\left(^{+0.28}_{-0.08}\right)$	0.25	$\left(^{+0.19}_{-0.05}\right)$	13.66	20.95
F15001+1433	6849.10	-220	(± 14)	283	(± 43)	0.46	$\left(^{+0.12}_{-0.07}\right)$	0.42	$\left(^{+0.11}_{-0.06}\right)$	13.67	20.97
⋯	6857.30	138	(± 11)	21	(± 19)	5.00	$\left(^{+\infty}_{-2.48}\right)$	0.08	$\left(^{+0.02}_{-0.04}\right)$	>13.58	>20.87
F17179+5444	6763.92	-52	(± 43)	232	(±100)	0.06	$\left(^{+0.10}_{-0.02}\right)$	0.80	$\left(^{+0.16}_{-0.03}\right)$	12.73	20.03
⋯	6772.13	312	(± 29)	179	(± 69)	0.47	$\left(^{+\infty}_{-0.14}\right)$	0.19	$\left(^{+0.32}_{-0.05}\right)$	>13.48	>20.78
F23233+2817	6571.65	-24	(± 26)	231	(± 77)	0.47	$\left(^{+\infty}_{-0.11}\right)$	0.10	$\left(^{+0.33}_{-0.02}\right)$	>13.59	>20.91
F23389+0300:N	6746.30	-206	(± 11)	300	(± 54)	0.24	$\left(^{+0.11}_{-0.02}\right)$	0.80	$\left(^{+0.18}_{-0.04}\right)$	13.41	20.81
F23389+0300:S	6753.76	-84	(± 31)	232	(± 84)	0.10	$\left(^{+\infty}_{-0.02}\right)$	0.97	$\left(^{+0.02}_{-0.00}\right)$	>12.93	>20.33
Seyfert 1s											
F07599+6508	6538.21	-10718	(± 53)	632	(±126)	0.50	$\left(^{+0.65}_{-0.12}\right)$	0.11	$\left(^{+0.15}_{-0.03}\right)$	14.05	21.35
⋯	6562.50	-9608	(±116)	1026	(±199)	4.09	$\left(^{+4.03}_{-2.12}\right)$	0.09	$\left(^{+0.09}_{-0.05}\right)$	15.17	22.47
⋯	6575.95	-8995	(± 95)	581	(±196)	0.39	$\left(^{+1.10}_{-0.13}\right)$	0.10	$\left(^{+0.28}_{-0.03}\right)$	13.91	21.20
⋯	6687.84	-3939	(± 10)	78	(± 33)	0.96	$\left(^{+6.40}_{-0.32}\right)$	0.06	$\left(^{+0.39}_{-0.02}\right)$	13.43	20.72
F11119+3257	6988.12	-1309	(± 3)	167	(± 8)	0.25	$\left(^{+0.05}_{-0.01}\right)$	1.00	$\left(^{+0.00}_{-0.00}\right)$	13.17	20.47
⋯	6995.27	-1002	(± 1)	23	(± 4)	2.84	$\left(^{+0.28}_{-0.17}\right)$	0.71	$\left(^{+0.07}_{-0.04}\right)$	13.37	20.67

Table 2—Continued

Name (1)	$\lambda_{1,c}$ (2)	Δv (3)		b (4)		$\tau_{1,c}$ (5)		C_f (6)		$N(\text{Na I})$ (7)	$N(\text{H})$ (8)
$\cdots$	7001.29	-744	($\pm$ 4)	121	($\pm$ 9)	0.17	$\left(^{+0.03}_{-0.02}\right)$	1.00	$\left(^{+0.00}_{-0.00}\right)$	12.86	20.15
Z11598−0114	$\cdots$	$\cdots$	$\cdots$	$\cdots$	$\cdots$	$\cdots$	$\cdots$	$\cdots$	$\cdots$	$\cdots$	$\cdots$
F12265+0219	$\cdots$	$\cdots$	$\cdots$	$\cdots$	$\cdots$	$\cdots$	$\cdots$	$\cdots$	$\cdots$	$\cdots$	$\cdots$
F12540+5708	5983.92	-8031	($\pm$ 3)	103	($\pm$ 9)	0.03	$\left(^{+0.00}_{-0.00}\right)$	0.71	$\left(^{+0.09}_{-0.03}\right)$	12.05	19.35
$\cdots$	6021.10	-6175	($\pm$ 0)	33	($\pm$ 1)	0.92	$\left(^{+0.03}_{-0.03}\right)$	0.33	$\left(^{+0.01}_{-0.01}\right)$	13.03	20.33
$\cdots$	6034.48	-5510	($\pm$ 0)	21	($\pm$ 6)	0.81	$\left(^{+0.09}_{-0.19}\right)$	0.28	$\left(^{+0.03}_{-0.06}\right)$	12.78	20.08
$\cdots$	6041.45	-5164	($\pm$ 4)	100	($\pm$ 8)	0.42	$\left(^{+0.06}_{-0.03}\right)$	0.61	$\left(^{+0.09}_{-0.05}\right)$	13.18	20.47
$\cdots$	6044.39	-5019	($\pm$ 11)	934	($\pm$ 45)	0.26	$\left(^{+0.03}_{-0.02}\right)$	0.17	$\left(^{+0.02}_{-0.01}\right)$	13.94	21.23
$\cdots$	6045.34	-4972	($\pm$ 2)	79	($\pm$ 8)	0.68	$\left(^{+0.06}_{-0.08}\right)$	0.84	$\left(^{+0.07}_{-0.10}\right)$	13.29	20.58
$\cdots$	6049.06	-4787	($\pm$ 21)	80	($\pm$ 30)	0.42	$\left(^{+0.50}_{-0.15}\right)$	1.00	$\left(^{+0.00}_{-0.00}\right)$	13.08	20.38
$\cdots$	6050.89	-4696	($\pm$ 23)	94	($\pm$ 22)	0.70	$\left(^{+0.18}_{-0.46}\right)$	1.00	$\left(^{+0.00}_{-0.00}\right)$	13.37	20.67
$\cdots$	6052.66	-4609	($\pm$ 9)	38	($\pm$ 34)	1.32	$\left(^{+0.28}_{-0.48}\right)$	0.64	$\left(^{+0.14}_{-0.23}\right)$	13.25	20.55
$\cdots$	6054.16	-4534	($\pm$ 8)	27	($\pm$ 20)	1.30	$\left(^{+0.13}_{-0.64}\right)$	0.84	$\left(^{+0.08}_{-0.42}\right)$	13.09	20.39
$\cdots$	6056.61	-4413	($\pm$ 1)	45	($\pm$ 3)	3.04	$\left(^{+0.18}_{-0.18}\right)$	0.74	$\left(^{+0.04}_{-0.04}\right)$	13.69	20.98
$\cdots$	6060.23	-4234	($\pm$ 0)	69	($\pm$ 2)	2.72	$\left(^{+0.08}_{-0.10}\right)$	0.69	$\left(^{+0.02}_{-0.02}\right)$	13.83	21.12
$\cdots$	6138.53	-386	($\pm$ 10)	149	($\pm$ 28)	0.14	$\left(^{+0.07}_{-0.01}\right)$	0.08	$\left(^{+0.04}_{-0.01}\right)$	12.86	20.16
F15462−0450	$\cdots$	$\cdots$	$\cdots$	$\cdots$	$\cdots$	$\cdots$	$\cdots$	$\cdots$	$\cdots$	$\cdots$	$\cdots$

Note. — Col.(2): Redshifted heliocentric wavelength, in vacuum, of the Na I D_1 $\lambda5896$ line; in Å. Col.(3): Velocity relative to systemic, in km s^{-1}; $\Delta v \equiv v_{comp} - v_{sys}$. Negative velocities are blueshifted. Components with $\Delta v < -50$ km s^{-1} and $|\Delta v| > 2\,\delta(\Delta v)$ are assumed to be outflowing. 1σ errors are listed in parentheses; these only include measurement uncertainties in v_{comp} (not v_{sys}). Col.(4): Doppler parameter, in km s^{-1}. 1σ measurement uncertainties are listed in parentheses. Col.(5): Central optical depth of the Na I D_1 $\lambda5896$ line; the optical depth of the D_2 line is twice this value. 1σ measurement uncertainties are listed in parentheses. Col.(6): Covering fraction of the gas. 1σ measurement uncertainties are listed in parentheses. Col.(7-8): Logarithm of column density of Na I and H, respectively, in cm^{-2}.

Table 3.   Outflow Properties

Name (1)	Δv_{maxN} (2)	Δv_{max} (3)	M (4)	dM/dt (5)	p (6)	dp/dt (7)	E (8)	dE/dt (9)
Seyfert 2s								
F05024−1941	-1547	-1669	9.19	2.47	50.46	36.43	58.33	44.32
F05189−2524	-402	-694	9.26	2.07	50.06	35.45	57.67	43.08
F08526+3720	-187	-400	>8.35	>0.93	>48.92	>34.00	>56.47	>41.55
F12278+3539	-546	-694	8.20	1.24	49.23	34.78	56.73	42.28
F13451+1232	-67	-364	8.75	0.88	48.87	33.51	57.04	41.67
F14478+3448	-487	-592	>7.99	>0.98	>48.97	>34.47	>56.40	>41.90
F14548+3349	-185	-240	8.21	0.78	48.77	33.85	55.81	40.89
F15001+1433	-220	-456	8.83	1.49	49.48	34.63	57.06	42.21
F23389+0300	-206	-456	>9.18	>1.69	>49.68	>34.75	>57.33	>42.39
Seyfert 1s								
F07599+6508	-9608	-11244	4.34	1.33	46.62	36.12	55.31	44.81
F11119+3257	-1002	-1448	3.73	-0.23	45.06	33.62	52.81	41.39
F12540+5708	-5019	-8117	4.41	1.09	46.38	35.56	54.75	43.93

Note. — Col.(2): Velocity of the highest column density gas in the outflow, Δv_{maxN}, in km s^{-1}. Col.(3): Maximum velocity in the outflow, $\Delta v_{max} \equiv \Delta v - \mathrm{FWHM}/2$, in km s^{-1}. Col.(4): Log of mass, in $M_{\odot}$. Col.(5): Log of mass outflow rate, in M$_{\odot}$ yr^{-1}. Col.(6): Log of momentum, in dyne s. Col.(7): Log of momentum outflow rate, in dyne. Col.(8): Log of total kinetic energy, in erg. Col.(9): Log of energy outflow rate, in erg s^{-1}.

Table 4.   Subsample Average Properties

Quantity (1)	IRGs (2)	low-z ULIRGs (3)	Seyfert 2s (4)	Seyfert 1s (5)
Number of Galaxies	35	30	20	6
Detection Rate (%)	42±8	80±7	45±11	50±20
Galaxy Properties				
z	$0.031^{+0.04}_{-0.02}$	$0.129^{+0.07}_{-0.04}$	$0.148^{+0.14}_{-0.07}$	$0.150^{+0.11}_{-0.06}$
$\log[L_{\rm IR}/L_\odot]$	11.36 ± 0.4	12.21 ± 0.2	12.24 ± 0.3	12.50 ± 0.2
SFR $(M_\odot\ \mathrm{yr}^{-1})$	40^{+55}_{-23}	225^{+95}_{-67}	118^{+151}_{-66}	164^{+91}_{-59}
Δv_{max} (km s^{-1})	301^{+145}_{-98}	408^{+224}_{-144}	456^{+330}_{-191}	8110^{+16291}_{-5414}
Δv_{maxN} (km s^{-1})	104^{+80}_{-45}	167^{+122}_{-70}	220^{+316}_{-130}	5023^{+11068}_{-3455}
$\log[N(\mathrm{Na\ I})/\mathrm{cm}^{-2}]$	13.8 ± 0.2	13.8 ± 0.4	13.5 ± 0.7	14.5 ± 0.8
$\log[N(\mathrm{H})/\mathrm{cm}^{-2}]$	21.2 ± 0.3	21.2 ± 0.4	20.9 ± 0.7	21.8 ± 0.8
$\log[M/M_\odot]$	8.8 ± 0.2	9.1 ± 0.3	8.8 ± 0.5	4.3 ± 0.4
$dM/dt\ (M_\odot\ \mathrm{yr}^{-1})$	17^{+20}_{-9}	42^{+82}_{-28}	18^{+50}_{-13}	12^{+73}_{-10}
$\log[p/\mathrm{dyne\ s}]$	49.2 ± 0.3	49.6 ± 0.5	49.2 ± 0.6	46.4 ± 0.8
$\log[dp/dt/\mathrm{dyne}]$	34.1 ± 0.5	34.7 ± 0.7	34.6 ± 0.9	35.6 ± 1.3
$\log[E/\mathrm{erg}]$	56.7 ± 0.4	57.2 ± 0.5	57.0 ± 0.7	54.8 ± 1.3
$\log[dE/dt/\mathrm{erg\ s}^{-1}]$	41.6 ± 0.6	42.2 ± 0.7	42.2 ± 1.0	43.9 ± 1.8
Component Properties				
τ	$1.06^{+1.4}_{-0.6}$	$0.85^{+2.4}_{-0.6}$	$0.27^{+0.7}_{-0.2}$	$0.69^{+1.6}_{-0.5}$
b (km s^{-1})	152^{+109}_{-64}	196^{+170}_{-91}	232^{+244}_{-119}	87^{+199}_{-61}
C_f	$0.37^{+0.2}_{-0.1}$	$0.40^{+0.5}_{-0.2}$	$0.42^{+0.5}_{-0.2}$	$0.67^{+1.2}_{-0.4}$

Note. — For most quantities we list the median and 1σ dispersions, under the assumption of a Gaussian distribution in the log of the quantity. For the detection rate errors, we assume a binomial distribution. Statistics for all quantities except z, $L_{\rm IR}$, and SFR are computed only for galaxies or velocity components with outflows.

Table 5.   Average Velocities by Spectral Type

Quantity	H II	LINER	Seyfert 2
$\Delta v_{max}(\text{km s}^{-1})$	-267 ± 133	-393 ± 194	-524 ± 439
$\Delta v_{maxN}(\text{km s}^{-1})$	-119 ± 95	-229 ± 135	-311 ± 457

Note. — For each quantity, we list the median and 1σ dispersions.

Table 6.　Comparing Velocity Distributions of Seyfert 2s and Starbursts

Samples	P(null,K-S)	P(null,Kuiper)
Δv_{max}		
IRGs vs. SB ULIRGs	0.11	0.28
SB ULIRGs vs. Sy2 ULIRGs	0.25	0.75
Sy2 ULIRGs vs. IRGs	0.04	0.21
H II vs. LINER	**<0.01**	**0.04**
LINER vs. Sy2	0.14	0.45
Sy2 vs. H II	0.05	0.25
Δv_{maxN}		
IRGs vs. SB ULIRGs	**0.01**	**0.09**
SB ULIRGs vs. Sy2 ULIRGs	0.13	0.16
Sy2 ULIRGs vs. IRGs	**0.01**	**0.09**
H II vs. LINER	0.07	0.27
LINER vs. Sy2	0.14	0.55
Sy2 vs. H II	**<0.01**	**0.01**
Doppler parameter		
IRGs vs. SB ULIRGs	0.19	0.55
SB ULIRGs vs. Sy2 ULIRGs	0.52	0.59
Sy2 ULIRGs vs. IRGs	0.14	0.33
H II vs. LINER	**0.02**	**<0.01**
LINER vs. Sy2	0.99	0.99
Sy2 vs. H II	0.13	0.06

Note. — P(null) is the probability that the two observed distributions arise from the same intrinsic distribution. Comparisons in which both values of P(null) are less than 0.10 are printed in bold face.

Table 7.   Emission- and Absorption-Line correlations

Axes (1)	Sample (2)	N (3)	$a \pm \delta a$ (4)	$P(r_p = 0)$ (5)	$P(r_s = 0)$ (6)
FWHM vs. Δv_{maxN}	all galaxies	38	-0.56 ± 0.07	0.00	0.01
FWHM vs. Δv_{maxN}	all galaxies with BELA	16	-0.62 ± 0.07	0.00	0.01
FWHM vs. Δv_{maxN}	Seyfert 2s with BELA	7	-0.64 ± 0.07	0.00	0.01

Note. — Col.(1): Variables to be fit. The line widths are of the [O III] λ5007 line. Col.(2): Subsample of galaxies in fit; full sample consists of all galaxies with neutral gas outflows and low-to-moderate resolution [O III] linewidths. BELA = blue emission-line asymmetry (§3.2). Col. (3): Number of nuclei in fit. Col.(4): Slope and 1σ error; $X = (a \pm \delta a)Y + Y_0$. Col.(5): Probability that Pearson's (parametric) correlation coefficient is zero. Col.(6): Probability that Spearman's (non-parametric) correlation coefficient is zero.